

**Anonymous Referee #1**

Style Definition: Normal

*This is an interesting study of the role of dust in droplet nucleation. Although some of the conclusions are compromised by neglect of droplet collision, I don't think those concerns need to be addressed in this study. There might even be value in neglecting droplet collisions, although that raises questions about the evaluation.*

We would like to thank the reviewer for his/her positive response. Indeed, as discussed in the text, the CDNC shown in this study is equal to the nucleated droplet number concentration before the collision and coalescence processes, which we acknowledge as an upper limit in clouds. This may result on the overestimation of CDNC in some areas. However, over polluted regions, where the model overestimates CDNC, the sensitivity of cloud albedo ( $R_c$ ) to CDNC is low. For typical values of cloud albedo ( $0.28 \leq R_c \leq 0.72$ )  $\Delta R_c = 0.075 \Delta \ln(\text{CDNC})$  (Seinfeld and Pandis, 2006). Therefore, Cloud albedo sensitivity to CDNC decreases with increasing CDNC. Based on the typical properties of stratus clouds, a 30% overestimation of CDNC results in 2.25% increase to cloud albedo and in a perturbation of  $-1.1 \text{ W m}^{-2}$  in the global mean cloud radiative forcing (Schwartz, 1996). Below is a point by point response to the reviewer's comments.

**Minor comments**

1. *Lines 65-58. Confusing text. I suggest instead "Reports of hygroscopic growth measurements of dust particles indicate solubility to be very low, so that activation of observed cloud condensation nuclei (CCN) has been attributed to soluble ions present in the particles".*

We adopted the reviewer's suggestion and changed the text accordingly.

2. *Line 71. Wouldn't the "fraction of soluble material on the particles" correspond to the soluble ions referred to above? Or is the critical distinction between soluble material within and on the surface of the particles? And between the fresh dust and aged dust? Perhaps even fresh dust is coated with soluble ions. This is not to say that adsorption or condensation of secondary soluble material are not important, but why neglect soluble material in the emitted dust. Surely some types of dust (clays?) must contain soluble material.*

Yes, in Line 71, the "fraction of soluble material on the particles" corresponds to the soluble ions referred in line 66. In this study we have implicitly taken into account the presence of soluble material in the freshly emitted dust by assuming that the emitted mineral particles are a mixture of inert material (i.e., bulk dust) with reactive components (i.e.,  $\text{Ca}^{2+}$ ,  $\text{Mg}^{2+}$ ,  $\text{K}^+$ , and  $\text{Na}^+$ ) that form soluble salts.

3. *Line 90. Start new paragraph with "Hatch".*

Done.

4. *Line 96. Start new paragraph with "Based".*

Done.

5. *Lines 117. Start new paragraph with “Soluble”, as the previous text describes mechanism while the following text describes conclusions above dust activity sampled in the atmosphere.*

Done.

6. *Line 143. Drop “Only”, as “few” implies it.*

Corrected.

7. *Line 159. I think you mean “aged dust can substantially deplete in-cloud supersaturation “, and replace “eventually” with “hence”.*

Corrected.

8. *Line 179. Replace “which “ with “that”.*

Done.

9. *Line 201. Replace “is” with “are”.*

Done.

10. *Section 3.1. This discussion never mentions the role of droplet collision in depleting droplet number concentration. Droplet activation is not the only process that determines droplet number concentration. Please consider the role of collision in your discussion, or show that it is not important (perhaps in thin warm clouds).*

In this study, droplet depletion by collision, coalescence and collection are not taken into account. Therefore, CDNC values presented in this section can be considered as an upper limit. This is now pointed out at the beginning of the section.

11. *Line 336. Are these in-cloud means?*

Yes, in this study, CDNC is referred to the number concentration of droplets nucleated in-cloud. We added this information in the text.

12. *Line 338. Replace “are” with “is”.*

Corrected.

13. Line 381. *The grid cell mean is typically less than 1 cm/s in global models. How large is the mean velocity over the central Asian deserts?*

The large scale updraft velocity over the central Asian deserts (e.g., over Gobi) ranges from  $-0.4 \text{ cm s}^{-1}$  to  $0.3 \text{ cm s}^{-1}$  throughout the year with an annual mean value of  $0.01 \text{ cm s}^{-1}$ .

14. Line 384. *Is 113 the global annual mean?*

Yes, it is the annual mean over all oceans.

15. Section 3.2 *I'm not sure what the purpose of this section is, since the aerosol and updraft velocity are not evaluated. Are you trying to show that the activation process is realistic, or just that droplet numbers are realistic? I'm not sure that you can achieve the former without validating the aerosol and updraft velocity too (or stratifying droplet number by aerosol and updraft velocity), and the latter is of limited value because EMAC neglects collision (as we learn later).*

Aerosol fields produced by EMAC have been evaluated against in-situ observations in previous studies (Pozzer et al., 2012; Tsimpidi et al., 2014; Karydis et al., 2016). The cloud droplet formation parameterization used in this work has been also extensively evaluated by comparing computations of CDNC and  $S_{max}$  and their sensitivity to aerosol properties against detailed numerical simulations of the activation process by a parcel-model (Betancourt and Nenes, 2014a). Furthermore, the cloud-averaged CDNC for stratocumulus clouds, which are described by EMAC, is well captured by the cloud droplet formation parameterization used in this study (Morales et al., 2011). Considering the influence of droplet collision and coalescence processes may, in part, reduce CDNC prediction biases, however, these processes are becoming important in the presence of clouds with substantial amount of drizzle. The purpose of this section is actually to provide a qualitative evaluation of the model's ability to capture the spatial and temporal variations of CDNC. The model is able to reproduce the increasing CDNC in air masses from clean marine regions to polluted marine and continental regions, though are biased somewhat high over the latter. However, a quantitative evaluation of the model is not currently feasible since the observations span over a decade (in contrast to the simulation which represents one year) and typically do not represent monthly means over  $1.9^\circ$  grid squares (as sampled from the model results). Furthermore, the

model tendency to overestimate the high values of CDNC has small impact on the overall cloud radiative forcing since cloud albedo sensitivity to CDNC decreases with increasing CDNC. Part of this discussion has been added in the revised manuscript.

*16. Line 408. In-cloud values?*

Yes, in this study, CDNC is referred to the number concentration of droplets nucleated in-cloud. We added this information in the text

*17. Line 441. Spatial and/or temporal variability?*

Here we refer to spatial variability. We have now clarified this in the text.

*18. Line 468. Now we finally learn that collision is neglected in the simulations. This should be noted before the comparisons are presented.*

In the revised manuscript, we have also included this information at the beginning of section 3.1.

*19. Line 493. This gets confusing. Please be explicit about whether you are referring to addition or subtraction of mineral dust.*

We refer to changes caused by the addition of mineral dust particles. This is now explicitly stated in the sentence.

*20. Line 502-503. This is the first time we learn about nudging. This should be reported in the experiment design.*

We included this information in section 2.1.

*21. Section 4.2. This is written very clearly and is quite interesting.*

We thank the reviewer for his/her positive comment.

*22. Line 607. Over over.*

Corrected.

*23. Lines 665-667. Should note again that the simulation neglects droplet collision.*

We noted again that we have neglected the collision and coalescence processes, which can lead to an overestimation of CDNC.

## ***Anonymous Referee #2***

*This work uses a suite of models (including the atmospheric chemistry model ECHAM5/MESy, MECCA, aerosol thermodynamics with ISORROPIA-II, and a series of other aerosol micro-physics subroutines) in order to explore, through numerical experiments, the potential global impact of wind-blown mineral dust in the number concentration of activated cloud droplets. Three mechanisms are explored in the paper: adsorption over insoluble dust particles, classical activation on particles with soluble coating, and a second order effect which involves interaction of the mineral cations in the dust particles with other inorganic aerosols. These mechanisms are explored through sensitivity simulations in which the model is run with/without the process under consideration. The paper is relevant and well written. The material presented is novel since it attempts to quantify potential impacts of a mechanism not previously considered. However, I think the discussion of the implications of these mechanisms should be performed in much more depth than what is done in the paper, and some substantial modifications in technical details are needed for the paper to be published. The difference between the conclusions found in this study and a previous work (Karydis et al 2011) should be made explicit.*

We thank the referee for the thoughtful review. Below are our responses to the issues raised.

### ***General comments***

- 1. No description of the cloud scheme utilized in the model is done. Therefore, it is not clear under which conditions is the activation parameterization triggered. Very little or no mention of cloud microphysics is done in the paper. The distribution of low level cloudiness in the model is not presented, which would be crucial to determine the actual extent of global impact of CDNC on aerosol-cloud-radiation interactions.*

The cloud scheme used in this study contains the original cloud process and cover routines from ECHAM5 and calculates the cloud microphysics by using the detailed two-moment liquid and ice-cloud microphysical scheme described in Lohmann and Ferrachat (2010), which enables a physically based treatment of aerosol–cloud interactions. This information has been added in section 2.1. The cloud droplet formation parameterization described in section 2.2 is only triggered when warm clouds are present (i.e., cloud water is present and temperature exceeds 269 K). We have also included this information in the revised manuscript. The distribution of the calculated low-level cloudiness has been added in Figure 2.

- 2. Although the paper is mainly focused on the impacts of dust on CDNC, no mention is done regarding the impact of dust on number concentration of aerosol particles that could activate. It would help in the interpretation of the results to know what the impact of switching dust emissions off is on the number and size of aerosol particles. A figure showing the changes caused by dust on the aerosol particles should be shown next to Figure 5.*

We do mention in section 4.1 that dust emissions increase the aerosol number concentration by more than  $5,000 \text{ cm}^{-3}$  over remote deserts. Following the reviewer's suggestion, we have also added a figure in the revised manuscript (Figure 6c) to show the changes in aerosol number concentration after switching on/off the mineral dust emissions. Due to the addition of mineral dust, total aerosol number concentration increases over the deserts, especially over remote deserts such as Taklimakan and Atacama, and decreases downwind of them and over polluted areas due to the coagulation of the coarse dust particles with the smaller anthropogenic aerosols.

3. *There is no mention in the paper about the geographic distribution of soluble and insoluble fractions in the dust modes predicted by the model. This would definitely help with the discussion and interpretation of the results. A map showing this distribution would help understanding the underlying processes.*

Thank you for the good suggestion; we have added a figure showing the spatial distribution of the insoluble fraction of particles.

4. *The paper does not explain how the CDNC shown in the maps is calculated. Are those grid-cell averages? Are those in-cloud values? Is this the value only after activation subroutine is called? Or are these values produced by the full cloud-microphysical scheme?*

CDNC values reported in the manuscript are referred to the number concentration of droplets nucleated in-cloud (i.e., right after the activation subroutine is called) and represent an upper limit since droplet depletion by collision, coalescence and collection are not taken into account. This information has been added in section 3.1

5. *No indication of the frequency of occurrence of liquid clouds at the level in the model is mentioned, nor that of the climatological cloud cover in those regions. If this is somehow included in the manuscript, the overall importance of dust on CDNC globally could be better assessed. The specifics of the annual average CDNC shown in the paper should be discussed and described in detail.*

The annual average low level cloud cover calculated by the EMAC model has been added in figure 2. While the calculated cloud cover over the main deserts is low (i.e., typically lower than 5%), CDNC is also sensitive to mineral dust emissions far from its sources and over areas with high cloud cover (e.g., over Europe and Eastern Asia). This is now discussed in the revised text.

6. *Some fundamental issues with the unified theory should be discussed by the authors in this manuscript. In particular the potential oversimplification of the activation process for insoluble particles with small soluble coatings (as could potentially be the case for dust particles). See specific comments.*

As discussed in detail below, we always assume that insoluble material (i.e., mineral dust) is expressed by the FHH terms. The aerosol hygroscopicity ( $\kappa$ ) of the soluble fraction is calculated according to the simple mixing rule. Then, based on the FHH terms, the  $\kappa$  hygroscopicity and the insoluble fraction ( $e_i$ ), the exponent  $x$  in Eq. 4 is calculated with a power law fit between  $S_g$  and  $D_{dry}$  as described in Kumar et al. (2011a).  $x$  lies between -0.86 for  $e_i=1$  and -1.5 for  $e_i=0$ .

7. *I suggest modifying some of the conclusions of the paper, since they can be overreaching. It doesn't seem that the paper actually "demonstrates" that the biases are substantial, or that this treatment is indeed correct. In fact, the authors acknowledge almost no sensitivity of CDNC to massive cuts in dust emissions, or hydrophilicity parameter, or on dust chemical composition. For example, I quote "By assuming drastic differences in the dust source and the dust hydrophilicity we find only small (~5%) changes in the average CDNC".*

The CDNC changes reported in the conclusion section are global averages. The global average changes of CDNC are small, mainly due to the negligible changes over the oceans and in some cases due to counteracting effects (i.e., opposite response of CDNC over the deserts and downwind of them). However, larger CDNC changes are calculated regionally (i.e., up to 30% over the deserts and 10% over highly polluted areas). This is now emphasized in the conclusions as well.

#### **Specific comments**

8. *Section 2.2. Line 265. It is not clear from the equations nor the references cited in the document, how can an exponent  $x = -3/2$  be obtained from equation (3) when there is insoluble material but no FHH terms. The -3/2 exponent arises from the fact that the whole volume of the particle contributes to the soluble material during the activation process. It is not explicit from the document what is the expression relating critical diameter and critical supersaturation when there is a substantial fraction of insoluble material (i.e., in equation 3, with no FHH terms, but a small amount of soluble material). The relations between dry aerosol size and critical supersaturation are severely modified when an insoluble core is present (see for example, Pruppacher and Klett, chapter 6, equations 6-37 to 6-42). Therefore, there is a possibility that one could see substantial changes in CDNC by simply improving the description of the relation between critical diameter and critical supersaturation for cases where there is an insoluble core (no FHH terms). This issue should be explored and discussed in the paper.*

We always assume that insoluble material (i.e., mineral dust) is expressed by the FHH terms. When mineral dust is present in the soluble modes,  $x$  is calculated by performing a power law fit between  $S_g$  and  $D_{dry}$  as described in Kumar et al. (2011a) and is given by:

$$x = x_{FHH} * \exp(\log(-1.5/x_{fhh}) * (1 - e_i) 0.1693 * \exp(-0.988\kappa))$$

$x$  lies between  $x_{FHH}$  for  $e_i=1$  and  $-1.5$  for  $e_i=0$ .  $e_i$  is the fraction of mineral dust in the mode,  $\kappa$  is the total aerosol hygroscopicity of the soluble fraction of the mode and the  $X_{FHH}$  depends on  $A_{FHH}$  and  $B_{FHH}$  used (Kumar et al., 2009b) and here is equal to  $-0.86$ .

Black carbon, which can exist in the soluble modes of our model after coagulation, is assumed to be part of the soluble material and affects the total aerosol hygroscopicity of the soluble fraction according to the simple mixing rule but not the exponent  $x$  of the soluble particle which, in the absence of mineral dust, is equal to  $-1.5$ .

9. *It would be convenient for the readers to see average values of CDNC, or average fractional changes printed in the global maps of figures 1, 2, 5, 6, 7 and 8*

This information has been added to the figures.

10. *The difference between results shown in Figure 5, and Figure 8c are not entirely clear to me. So figure 5 has no mineral dust emissions, and Figure 8c, was performed with 50% aerosol emissions compared to base case? So in the case of no emissions, there is a net decrease in CDNC, but when there is only a 50% decrease in the emission load there is an increase in CDNC?*

They are just illustrated vice versa. Figure 5 depicts the CDNC change after including mineral dust emissions (increasing mineral dust) while figure 8c depicts the CDNC change after assuming 50% less dust emissions (decreasing mineral dust). In both cases CDNC decreases with increasing mineral dust.

11. *Line 712. Should it read "insensitive"?*

Changed.

12. *Figure 2. Are these values grid-cell averages? Or are they in-cloud values only?*

They are in-cloud values. We have added this information in figures 1, 2 and 3.

13. *From figure 8, it seems that BFHH parameter has a larger (or at least comparable) impact to reducing mineral dust emissions by 50%? This should be discussed in much more detail. As mentioned above, perhaps showing the net impact that the 50% reduction in dust emissions has on aerosol number concentration would be helpful in the interpretation of the results.*

In both simulations, the sensitivity of CDNC is dominated by the changes in the calculated critical supersaturation of the particle as well as the exponent  $x$  in Eq. (4). Reducing the dust emissions by 50% results in an increase of aerosol number concentration by less than 10% downwind of deserts and over polluted regions (which mostly control the global average change of CDNC). However, the insoluble fraction of particles over these regions decreases by 40% which significantly affects, through changes in equilibrium water vapor supersaturation (Eq. 3), the “CCN spectrum” (Eq. 4). Similarly, increasing the hydrophilicity of the dust particles by changing the  $B_{FHH}$  parameter, directly affects the equilibrium supersaturation and the “CCN spectrum” through changes in the exponent  $x$ . These issues are discussed in sections 5.2 and 5.3.

14. *Similarly, the paper shows very little sensitivity of CDNC to dust chemical composition, but relatively high sensitivity to the BFHH parameter. However, it is reasonable to believe that the FHH parameters are linked to the chemical composition of the mineral dust particles. Therefore, some discussion should be included regarding the relationship between the FHH theory parameters and dust chemical composition, and the potential impacts it could have in the simulations.*

The sensitivity test presented in section 5.1 describes the effect of the chemical composition of dust on the results only due to changes on the thermodynamic interactions with inorganic anions. The FHH parameters describe the hydrophilicity of fresh dust. Their values are determined to reproduce the measured CCN activity of the dust samples. Kumar et al. (2011b) tested the CCN activity of aerosols dry generated from clays, calcite, quartz, and desert soil samples from Northern Africa, East Asia/China, and Northern America. They found that  $B_{FHH}$ , which strongly affects the equilibrium curve, varied from 1.12 to 1.30 (i.e.,  $\pm 10\%$  from 1.2 which is the value used in our base case simulation). Therefore, the sensitivity test presented in section 5.2, where we assumed 10% lower  $B_{FHH}$ , can represent the potential impacts on the results due the simplification of using a globally uniform set of FHH parameters to describe the hydrophilicity of mineral dust independently of its source and composition. Our results indicate that changes in the hydrophilicity of the freshly emitted dust, due to the variability of its composition with source region, can have an important impact on the calculated CDNC. This is now emphasized in section 5.2.



# Global impact of mineral dust on cloud droplet number concentration

Vlassis A. Karydis<sup>1</sup>, Alexandra P. Tsimpidi<sup>1</sup>, Sara Bacer<sup>1</sup>, Andrea Pozzer<sup>1</sup>,  
Athanasios Nenes<sup>2,3,4</sup> and Jos Lelieveld<sup>1,5</sup>

<sup>1</sup>Max Planck Institute for Chemistry, Mainz, 55128, DE

<sup>2</sup>Georgia Institute of Technology, Atlanta, GA, 30332, USA

<sup>3</sup>National Observatory of Athens, Palea Penteli, 15236, GR

<sup>4</sup>Foundation for Research and Technology Hellas, Patras, 26504, GR

<sup>5</sup>The Cyprus Institute, Nicosia, 1645, CY

## Abstract

The importance of wind-blown mineral dust for cloud droplet formation is studied by considering *i*) the adsorption of water on the surface of insoluble particles, *ii*) the particle coating by soluble material (~~due to~~ atmospheric aging) which augments cloud condensation nuclei (CCN) activity, and *iii*) the effect of dust on inorganic aerosol concentrations through thermodynamic interactions with mineral cations. The ECHAM5/MESSy Atmospheric Chemistry (EMAC) model is used to simulate the composition of global atmospheric aerosol; ~~while~~ the ISORROPIA-II thermodynamic equilibrium model treats the interactions of  $K^+$ - $Ca^{2+}$ - $Mg^{2+}$ - $NH_4^+$ - $Na^+$ - $SO_4^{2-}$ - $NO_3^-$ - $Cl^-$ - $H_2O$  aerosol with gas-phase inorganic constituents. Dust is considered a mixture of inert material with reactive minerals; ~~and its~~ emissions are calculated online by taking into account the soil particle size distribution and chemical composition of different deserts worldwide. The impact of dust on droplet formation is treated through the “unified dust activation parameterization” that considers the inherent hydrophilicity from adsorption and acquired hygroscopicity from soluble salts during aging. Our simulations suggest that the presence of dust increases cloud droplet number concentrations (CDNC) over major deserts (e.g., up to 20% over the Sahara and Taklimakan Deserts) and decreases CDNC over polluted areas (e.g., up to 10% over southern Europe and 20% over northeastern Asia). This leads to a global net decrease of CDNC by 11%. The adsorption activation of insoluble aerosols and the mineral dust chemistry are shown to be equally important for the cloud droplet formation over the main ~~desserts~~deserts, e.g., ~~by considering~~ these effects increase CDNC ~~increases~~ by 20% over the Sahara. Remote from deserts the application of adsorption theory is critically important since the increased water uptake by the large aged dust particles (i.e., due to the added hydrophilicity by the soluble coating) reduce the maximum

39 | supersaturation and thus ~~the~~ cloud droplet formation from the relatively smaller  
40 anthropogenic particles (e.g., CDNC decreases by 10% over southern Europe and  
41 20% over northeastern Asia by applying adsorption theory). The global average  
42 CDNC decreases by 10% by considering adsorption activation, while changes are  
43 negligible when accounting for the mineral dust chemistry. Sensitivity simulations  
44 indicate that CDNC is also sensitive to the mineral dust mass and inherent  
45 hydrophilicity, and not to the chemical composition of the emitted dust.

46

## 47 | 1. Introduction

48 Atmospheric aerosols from anthropogenic and natural sources adversely affect  
49 human health and influence the Earth's climate, both directly and indirectly  
50 (Haywood and Boucher, 2000; Lohmann and Feichter, 2005; Andreae and Rosenfeld,  
51 2008; IPCC, 2013; Kushta et al., 2014; Lelieveld et al., 2015). The direct climate  
52 effect refers to the influence of aerosols on the radiative budget of Earth's atmosphere  
53 by scattering and absorbing solar radiation (Seinfeld and Pandis, 2006). The indirect  
54 effects include the ability of aerosols to affect the cloud optical thickness and  
55 scattering properties of clouds (Twomey, 1974) as well as the cloud lifetime and  
56 precipitation (Albrecht, 1989). The scientific interest in aerosol-cloud-climate  
57 interactions initially focused on anthropogenic pollutants (e.g., sulfate) and to a lesser  
58 extent on naturally emitted aerosols (e.g., sea salt). However, among atmospheric  
59 aerosols, mineral dust is of particular importance since it is globally dominant in  
60 terms of mass concentration in the atmosphere (Grini et al., 2005; Zender and Kwon,  
61 2005) and can influence cloud and precipitation formation (Levin et al., 2005; Yin  
62 and Chen, 2007; Karydis et al., ~~2011~~2011a; Rosenfeld et al., 2011; Kallos et al.,  
63 2014). Additionally, dust alone is responsible for more than 400,000 ~~premature~~ deaths  
64 attributable to air pollution per year (Giannadaki et al., 2014).

65 Freshly emitted dust is considered insoluble. Reports of hygroscopic growth  
66 measurements of dust particles indicate solubility to be very low, ~~which together with~~  
67 ~~these that activation of~~ observed cloud condensation nuclei (CCN) has been  
68 attributed to soluble ions present in the particles (Gustafsson et al., 2005; Herich et al.,  
69 2009; Koehler et al., 2009; Garimella et al., 2014). Chemistry – climate models  
70 (CCMs) typically use Köhler theory to describe droplet formation from dust, which  
71 assumes that the CCN activity depends solely on their curvature effect and the  
72 fraction of soluble material on the particle (Smoydzin et al., 2012). However, mineral

Field Code Changed

73 dust can adsorb water which results in a surface film of water with reduced activity  
74 (Sorjamaa and Laaksonen, 2007), and promote the formation of cloud droplets at  
75 cloud-relevant supersaturation, even of freshly emitted and chemically unprocessed  
76 dust particles (Sorjamaa and Laaksonen, 2007; Kumar et al., 2009a). Kumar et al.  
77 (2009a) emphasized the importance of including water adsorption effects in  
78 describing the hygroscopic growth of mineral aerosols, which was then included in a  
79 droplet formation parameterization (~~Kumar et al. (2009b)~~(Kumar et al., 2009b) for use  
80 in models. Evidence on the importance of adsorption activation of dust particles is  
81 discussed in Kumar et al. (2011b; 2011a) for dry- and wet-generated clays and  
82 mineral dusts representative of major regional dust sources (North Africa, East Asia  
83 and North America). Adsorption activation was also found to be important for  
84 volcanic ashes (Latham et al., 2011). The observed hygroscopicity could not be  
85 attributed to the soluble ions present, but rather to the strong water vapor adsorption  
86 on the particle surface. Furthermore, the surface fractal dimension derived from dust  
87 and ash critical supersaturation data agrees well with previous methods based on  
88 measurements of nitrogen adsorption, which contribute strong evidence for adsorption  
89 effects on water activity and droplet activation (Laaksonen et al., 2016), despite  
90 concerns raised by Garimella et al. (2014) on multiple charging effects on the work of  
91 Kumar et al. (2011b).

92 Hatch et al. (2014) provided an alternative approach for parameterizing CCN  
93 activation of fresh atmospheric mineral aerosol. This approach was based on  
94 experimental water adsorption measurements on mineral clays compared to CCN  
95 measurements used by Kumar et al. (2011b), which require corrections for multiply  
96 charged particles and non-sphericity. Despite differences in the adsorption parameters  
97 reported from the above two studies, the adsorption derived CCN activities were quite  
98 similar and in excellent agreement.

99 Based on these findings, Karydis et al. (~~2011~~2011a) integrated the Kumar et al.  
100 (2009b) parameterization into the Global Modeling Initiative (GMI) chemical  
101 transport model (Conside et al., 2005) and found that insoluble mineral dust can  
102 contribute up to 24% of the cloud droplet number downwind of arid areas.  
103 Subsequently, the Kumar et al. (2009b) parameterization has been integrated in a  
104 number of global and regional models and applied to investigate the impact of mineral  
105 dust on warm cloud formation (Bangert et al., 2012; Karydis et al., 2012; Gantt et al.,  
106 2014; Zhang et al., 2015).

Field Code Changed

107 Soluble inorganic ions like ~~Ca<sup>+2</sup>, Mg<sup>+2</sup>, Ca<sup>2+</sup>, Mg<sup>2+</sup>~~, Na<sup>+</sup>, and K<sup>+</sup> that exist on the  
108 surface of mineral dust particles can participate in heterogeneous chemical reactions  
109 with acids such as HNO<sub>3</sub> and HCl. Furthermore, dust particles can provide reaction  
110 sites for the SO<sub>2</sub> oxidation into H<sub>2</sub>SO<sub>4</sub>. These processes result in the coating of dust  
111 particles by soluble material, which augments the hygroscopicity of dust and therefore  
112 its ability to act as CCN (Kelly et al., 2007). On the other hand, highly oxidized,  
113 soluble organic species, particularly including carboxylic acid groups (e.g., oxalic  
114 acid), can interact with particles dominated by di-valent salts (e.g., CaCl<sub>2</sub>) and  
115 strongly decrease their hygroscopicity (Drozd et al., 2014). Due to their relatively  
116 large size, chemically aged dust particles can act as giant CCN, enhancing  
117 precipitation as they efficiently collect moisture and grow at the expense of smaller  
118 droplets (Feingold et al., 1999; Levin et al., 2005). In addition, giant CCN compete  
119 with the submicron particles for water vapor, potentially reducing supersaturation and  
120 cloud droplet formation (Barahona et al., 2010; Betancourt and Nenes, 2014b;  
121 Betancourt and Nenes, 2014a).

Field Code Changed

Field Code Changed

122 Soluble coatings on dust are mostly evident in the atmosphere after long-range  
123 transport of dust plumes. Anthropogenic NO<sub>3</sub><sup>-</sup> and SO<sub>4</sub><sup>2-</sup> mainly contribute to the  
124 chemical aging of dust over continents while sea salt derived Cl<sup>-</sup> is more important  
125 over oceans (Sullivan et al., 2007; Fountoukis et al., 2009; Dall'Osto et al., 2010;  
126 ~~Tobo et al., 2010; Karydis et al., 2011b~~; Bougiatioti et al., 2016b; Weber et al., 2016).

Field Code Changed

Field Code Changed

Field Code Changed

127 Apart from the gas phase composition, the chemical processing of dust also depends  
128 on its chemical composition and thus on the source region (Sullivan et al., 2009;  
129 ~~Karydis et al., 2016~~). Several studies have revealed that Saharan dust can be

Field Code Changed

Field Code Changed

130 efficiently transported over the Mediterranean basin where it can acquire significant  
131 soluble coatings (mostly sea salt and sulfate) resulting in the enhancement of its  
132 hygroscopicity and CCN activity (Wurzler et al., 2000; Falkovich et al., 2001;  
133 ~~Smoydzin et al., 2012; Abdelkader et al., 2015~~). Twohy et al. (2009) have shown that

Field Code Changed

Field Code Changed

Field Code Changed

134 Saharan dust often acts as CCN over the eastern North Atlantic and significantly  
135 contributes to cloud formation west of Africa. Begue et al. (2015) analyzed a case of  
136 possible mixing of European pollution aerosols with Saharan dust transported over  
137 northern Europe, and found that aged Saharan dust was sufficiently soluble to impact  
138 the hygroscopic growth and cloud droplet activation over the Netherlands. Asian dust  
139 has also been reported to have a considerable impact on cloud formation after being  
140 transported over long distances and mixed with soluble materials (Perry et al., 2004;

Field Code Changed

141 Roberts et al., 2006; Sullivan et al., 2007; Ma et al., 2010; Stone et al., 2011;  
142 Yamashita et al., 2011).

143 Despite the importance of mineral dust aerosol chemistry for accurately predicting  
144 the aerosol hygroscopicity changes that accompany these reactions, most  
145 thermodynamic models used in global studies lack a realistic treatment of crustal  
146 species, e.g., assuming that mineral dust is chemically inert (Liao et al., 2003; Martin  
147 et al., 2003; Koch et al., 2011; Leibensperger et al., 2011). ~~Only few~~ Few global  
148 studies have accounted for the thermodynamic interactions of crustal elements with  
149 inorganic aerosol components (Feng and Penner, 2007; Fairlie et al., 2010; Xu and  
150 Penner, 2012; Hauglustaine et al., 2014; Karydis et al., 2016). Most of these models  
151 either neglect the impact of dust on cloud droplet formation or apply simplified  
152 assumptions about the CCN activity of dust, e.g., they convert “hydrophobic” dust to  
153 “hydrophilic” dust by applying a constant  $\kappa$ -hygroscopicity (e.g., 0.1) and use Köhler  
154 theory to describe cloud droplet activation. However, accounting for both the inherent  
155 hydrophilicity of dust and the acquired hygroscopicity from soluble salts could  
156 improve the predictive capability of CCMs. For this purpose, Kumar et al. (2011a)  
157 presented a “unified dust activation framework” (UAF) to treat the activation of dust  
158 with substantial amounts of soluble material by considering the effects of adsorption  
159 (due to the hydrophilicity of the insoluble core) and absorption (due to the  
160 hygroscopicity of the soluble coating) on CCN activity. Karydis et al. (~~2011~~2011a)  
161 provided a first estimate of aged dust contribution to global CCN and cloud droplet  
162 number concentration (CDNC) by using the UAF. They found that coating of dust by  
163 hygroscopic salts can cause a twofold enhancement of its contribution to CCN. On the  
164 other hand, aged dust can ~~be~~ substantially ~~depleted due to~~ deplete in-cloud  
165 supersaturation and ~~eventually~~ hence reduce the CDNC. Bangert et al (2012)  
166 investigated the impact of Saharan dust on cloud droplet formation over western  
167 Europe and found only a slight increase in calculated CDNC. However, these studies  
168 did not include thermodynamic interactions of mineral dust with sea salt and  
169 anthropogenic pollutants. Instead, a prescribed fraction of mineral dust that is coated  
170 with ammonium sulfate was used to represent the aged dust.

171 The present work aims at advancing previous studies ~~on~~of dust influences ~~on~~fon  
172 cloud droplet formation by comprehensively considering *i*) the adsorption of water on  
173 the surface of insoluble dust particles, *ii*) the coating of soluble material on the surface  
174 of mineral particles which augments their CCN activity, and, *iii*) the effects of dust on

Field Code Changed

175 the inorganic soluble fraction of dust through thermodynamic interactions of semi-  
176 volatile inorganic species and sulfate with mineral cations. The ECHAM5/MESSy  
177 Atmospheric Chemistry (EMAC) model (Jöckel et al., 2006) is used to simulate  
178 aerosol processes, while the “unified dust activation framework” (Karydis et al.,  
179 ~~2014~~2011a; Kumar et al., 2011a) is applied to calculate the CCN spectra and droplet  
180 number concentration, by explicitly accounting for the inherent hydrophilicity from  
181 adsorption and acquired hygroscopicity from soluble salts by dust particles from  
182 atmospheric aging. Mineral dust chemistry has been taken into account by using the  
183 thermodynamic equilibrium model ISORROPIA II (Fountoukis and Nenes, 2007).  
184 Dust emissions are calculated online by an advanced dust emission scheme ~~which that~~  
185 accounts for the soil particle size distribution (Astitha et al., 2012) and chemical  
186 composition (Karydis et al., 2016) of different deserts worldwide. The sensitivity of  
187 the simulations to the emitted dust aerosol load, the mineral dust chemical  
188 composition and the inherent hydrophilicity of mineral dust is also considered.

Field Code Changed

Field Code Changed

Field Code Changed

## 189 190 2. Model Description

### 191 192 2.1 EMAC Model

193 We used the ECHAM5/MESSy Atmospheric Chemistry (EMAC) model (Jöckel et  
194 al., 2006) which uses the Modular Earth Submodel System (MESSy2) (Jöckel et al.,  
195 2010) to connect submodels that describe the lower and middle atmosphere processes  
196 with the 5th generation European Centre - Hamburg (ECHAM5) general circulation  
197 model (GCM) as a dynamical core (Röckner et al., 2006). EMAC has been  
198 extensively described and evaluated against in-situ observations and satellite  
199 retrievals (de Meij et al., 2012; Pozzer et al., 2012; ~~Tsimpidi~~Karydis et al., ~~2014~~2016;  
200 ~~Karydis~~Tsimpidi et al., ~~2016~~2017). The spectral resolution of the EMAC model used  
201 in this study is T63L31, corresponding to a horizontal grid resolution of  
202 approximately  $1.9^\circ \times 1.9^\circ$  and 31 vertical layers between the surface and 10 hPa (i.e. 25  
203 km altitude). ~~The model dynamics has been weakly nudged (Jeuken et al., 1996)~~  
204 ~~towards the analysis data of the European Centre for Medium-Range Weather~~  
205 ~~Forecasts (ECMWF) operational model (up to 100 hPa) to represent the actual day-to-~~  
206 ~~day meteorology in the troposphere.~~ EMAC is applied for 2 years covering the period  
207 2004-2005 and the first year is used as spin-up.

Field Code Changed

Field Code Changed

Field Code Changed

Field Code Changed

208 EMAC simulates the gas phase species through the MECCA submodel (Sander et  
209 al., 2011). Aerosol microphysics are calculated by the GMXe module (Pringle et al.,  
210 2010). The organic aerosol formation and chemical aging ~~is~~are calculated by the  
211 ORACLE submodel (Tsimpidi et al., 2014). The CLOUD submodel (Röckner et al.,  
212 2006) ~~calculates the cloud cover as well as cloud micro physics and precipitation of~~  
213 ~~large scale clouds (i.e., excluding convective clouds).~~ calculates the cloud cover as  
214 well as cloud microphysics and precipitation of large scale clouds (i.e., excluding  
215 convective clouds). The cloud microphysical processes are computed by using the  
216 detailed two-moment liquid and ice-cloud microphysical scheme described in  
217 Lohmann and Ferrachat (2010), which enables a physically based treatment of  
218 aerosol–cloud interactions. The wet and dry deposition are calculated by the SCAV  
219 (Tost et al., 2006) and the DRYDEP (Kerkweg et al., 2006) sub-models.

220 The inorganic aerosol composition is computed with the ISORROPIA-II  
221 (<http://isorro피아.eas.gatech.edu>) thermodynamic equilibrium model (Fountoukis and  
222 Nenes, 2007) with updates as discussed in Capps et al. (2012). ISORROPIA-II  
223 calculates the gas-liquid-solid equilibrium partitioning of the  $K^+$ - $Ca^{2+}$ - $Mg^{2+}$ - $NH_4^+$ -  
224  $Na^+$ - $SO_4^{2-}$ - $NO_3^-$ - $Cl^-$ - $H_2O$  aerosol system. Potassium, calcium, magnesium, and  
225 sodium are assumed to exist in the form of  $Ca(NO_3)_2$ ,  $CaCl_2$ ,  $CaSO_4$ ,  $KHSO_4$ ,  $K_2SO_4$ ,  
226  $KNO_3$ ,  $KCl$ ,  $MgSO_4$ ,  $Mg(NO_3)_2$ ,  $MgCl_2$ ,  $NaHSO_4$ ,  $Na_2SO_4$ ,  $NaNO_3$ ,  $NaCl$  in the solid  
227 phase and  $Ca^{2+}$ ,  $K^+$ ,  $Mg^{2+}$ ,  $Na^+$  in the aqueous phase. More details about the EMAC  
228 model set up used in this study can be found in Karydis et al. (2016).

229

## 230 2.2 CCN Activity and Cloud Droplet Formation Parameterization

231 The cloud droplet formation parameterization is triggered only when warm clouds  
232 are present (i.e., cloud water is present and temperature exceeds 269 K). The  
233 equilibrium supersaturation,  $s$ , over the surface of a water droplet containing a solute  
234 particle (i.e., without any insoluble material present) is calculated using the  
235 hygroscopicity parameter,  $\kappa$ , based on  $\kappa$ -Köhler theory (Petters and Kreidenweis,  
236 2007):

237

$$s = \frac{4\sigma M_w}{RT\rho_w D_p} - \frac{D_{dry}^3 \kappa}{D_p^3} \quad (1)$$

Field Code Changed

Field Code Changed

Field Code Changed

Field Code Changed

Formatted: Font color: Auto

Formatted: Font color: Black, Pattern: Clear (White)

Field Code Changed

Field Code Changed

Field Code Changed

238 where  $D_{dry}$  is the dry CCN diameter,  $D_p$  is the droplet diameter,  $\sigma$  is the CCN  
 239 surface tension at the point of activation,  $\rho_w$  is the water density,  $M_w$  is the molar mass  
 240 of water,  $R$  is the universal gas constant, and  $T$  is the average column temperature.

Formatted: Font: Italic

241 For insoluble particles (e.g., pristine mineral dust), the multilayer Frenkel-Halsey-  
 242 Hill (FHH) adsorption isotherm model (Sorjamaa and Laaksonen, 2007) is used,  
 243 which contains two adjustable parameters ( $A_{FHH}$  and  $B_{FHH}$ ) that describe the  
 244 contribution of water vapor adsorption on CCN activity. In this case, the equation  
 245 describing the equilibrium supersaturation over the surface of a water droplet is given  
 246 by (Kumar et al., 2009b):

Field Code Changed

$$247 \quad s = \frac{4\sigma M_w}{RT \rho_w D_p} - A_{FHH} \left( \frac{D_p - D_{dry}}{2D_w} \right)^{-B_{FHH}} \quad (2)$$

Field Code Changed

248 where  $D_w$  is the diameter of a water molecule. The adsorption parameter  $A_{FHH}$   
 249 represents the interactions between the first water monolayer and the dust surface.  
 250  $B_{FHH}$  expresses the long range interactions of additional adsorbed water layers with  
 251 the dust surface. Kumar et al. (2011b) tested a wide range of fresh unprocessed  
 252 regional dust samples and minerals and found that one set of the FHH parameters  
 253 ( $A_{FHH} = 2.25 \pm 0.75$ ,  $B_{FHH} = 1.20 \pm 0.10$ ) adequately reproduces the measured CCN  
 254 activity for all dust types considered.

Field Code Changed

255 To account for the coating of soluble material on the surface of mineral dust, the  
 256 “unified activation framework” (Karydis et al., 2011a; Kumar et al., 2011a) is  
 257 used, which describes the water vapor supersaturation over an aerosol particle  
 258 consisting of insoluble core with a soluble coating:

Field Code Changed

Field Code Changed

$$259 \quad s = \frac{4\sigma M_w}{RT \rho_w D_p} - \frac{\varepsilon_s D_{dry}^3 \mathcal{K}}{(D_p^3 - \varepsilon_i D_{dry}^3)} - A_{FHH} \left( \frac{D_p - \varepsilon_i^{1/3} D_{dry}}{2D_w} \right)^{-B_{FHH}} \quad (3)$$

260 where  $\varepsilon_i$  is the insoluble volume fraction and  $\varepsilon_s$  is the soluble volume fraction. Eq. 3  
 261 takes into account both the inherent hydrophilicity from adsorption expressed in the  
 262 third term of the equation and the acquired hygroscopicity from soluble salts by dust  
 263 particles expressed in the second term of the equation. The first term accounts for the  
 264 Kelvin effect. Noting that for a complete insoluble dust particle, i.e., as  $\varepsilon_s \rightarrow 0$  and  
 265  $\varepsilon_i \rightarrow 1$ , the UAF approaches FHH theory (Eq. 2). Black carbon (BC) is not expressed

266 by the FHH terms in eq. 3. Instead, BC is assumed to have zero hygrscopicity and  
267 affects  $\kappa$  in eq. 3 according to the simple mixing rule.

268 Calculation of CDNC is carried out in two conceptual steps, one involving the  
269 determination of the “CCN spectrum” (i.e., the number of CCN that can activate to  
270 form droplets at a certain level of supersaturation), and another one determining the  
271 maximum supersaturation,  $s_{\max}$ , that develops in the ascending cloudy air parcels used  
272 to represent droplet formation in EMAC. The CDNC is then the value of the CCN  
273 spectrum at  $s_{\max}$ .

274 The “CCN spectrum”,  $F^s(s)$ , is computed following Kumar et al. (2009b) and  
275 assumes that particles can be described either by KT or FHH theory.  $F^s(s)$  for an  
276 external mixture of lognormal particle size distributions is given by:

$$277 \quad F^s(s) = \int_0^s n^s(s) ds = \sum_{i=1}^{n_m} \frac{N_i}{2} \operatorname{erfc} \left[ -\frac{\ln \left( \frac{s_{g,i}}{s} \right)}{x\sqrt{2} \ln(\sigma_i)} \right] \quad (4)$$

278 where  $s$  is the level of water vapor supersaturation,  $n^s(s)$  is the critical  
279 supersaturation distribution,  $s_{g,i}$  is the critical supersaturation of the particle with a  
280 diameter equal to the geometric mean diameter of the mode  $i$ ,  $\sigma_i$  is the geometric  
281 standard deviation for the mode  $i$ , and  $x$  is an exponent that depends on the  
282 activation theory used. For modes following Köhler theory,  $x = -\frac{3}{2}$  (Fountoukis and

283 Nenes, 2005), while for insoluble particles following FHH theory,  $x$  depends on  
284  $A_{FHH}$  and  $B_{FHH}$  (Kumar et al., 2009b). ~~In the case of UAF (i.e.,  $x=0.86$  for  $A_{FHH}$~~

285  ~~$=2.25$  and  $B_{FHH}=1.20$  used here). In the case of UAF,  $x$  lies between the KT and~~

286 FHH-AT limits, and is determined from Eq. (3) by performing a power law fit  
287 between  $s_g$  and  $D_{dry}$  as described in Kumar et al. (2011a). The calculation of  $s_g$

288 involves determining the maximum of the relevant equilibrium curve in equilibrium

289 with the surrounding water vapor ( $\left. \frac{ds}{dD_p} \right|_{D_p=D_g} = 0$  in Eqs. 1-3). Once  $D_g$  is determined,

290 it can be substituted in Eqs. 1-3 to obtain  $s_g$ .

Field Code Changed

Field Code Changed

Field Code Changed

291 The maximum supersaturation,  $s_{\max}$ , in the ascending parcel is calculated from an  
 292 equation that expresses the supersaturation tendency in cloudy air parcels, which at  
 293 the point of maximum supersaturation becomes (Nenes and Seinfeld, 2003; Barahona  
 294 and Nenes, 2007)

$$295 \quad \frac{2aV}{\pi\gamma\rho_w} - Gs_{\max}I(0, s_{\max}) = 0 \quad (5)$$

296 where  $V$  is the updraft velocity (i.e., not including convection) calculated online by  
 297 assuming that the sub-grid vertical velocity variability is dominated by the turbulent  
 298 transports and by choosing the root-mean-square value of the GCM model-generated  
 299 turbulent kinetic energy ( $TKE$ ) as a measure. Based on this assumption, the in-cloud  
 300 updraft velocity can be expressed as  $V = \bar{V} + 0.7\sqrt{TKE}$ , where  $\bar{V}$  is the GCM-resolved large scale updraft velocity (Lohmann et al., 1999a;  
 301 Lohmann et al., 1999b). Following Morales and Nenes (2010),  $V$  can be considered as  
 302 a “characteristic updraft velocity” which yields CDNC value representative of  
 303 integration over a probability density function (PDF) of updraft velocity. Morales and  
 304 Nenes (2010) have shown that this assumption applies well to large scale clouds (i.e.,  
 305 stratocumulus), which are the type of clouds described by the CLOUD sub-model in  
 306 EMAC.  $a, \gamma, G$  in Eq. (5) are parameters defined in Nenes and Seinfeld (2003).  
 307  $I(0, s_{\max})$  is the “condensation integral” which expresses the condensational depletion  
 308 of supersaturation upon the growing droplets at the point of  $s_{\max}$  in the cloud updraft.  
 309 It is expressed as the sum of two terms:

$$312 \quad I(0, s_{\max}) = I_K(0, s_{\max}) + I_{FHH}(0, s_{\max}) \quad (6)$$

314 The first term on the right hand side of Eq. (6),  $I_K(0, s_{\max})$ , describes the contribution  
 315 from particles that follow the Köhler theory and is calculated using the revisited  
 316 population splitting approach of Betancourt and Nenes (2014a). The second term,  
 317  $I_{FHH}(0, s_{\max})$ , represents the contribution of freshly emitted or aged dust particles to  
 318 the condensation integral and is represented in Kumar et al. (2009b) and Karydis et al.  
 319 (2011a). Once  $s_{\max}$  is determined by numerically solving Eq. (5), the number of  
 320 cloud droplets that form in the parcel,  $N_d$ , is obtained from the “CCN spectrum” (Eq.

Field Code Changed

321 (4)) computed for  $s_{\max}$ , i.e.,  $N_d = F(s_{\max})$ . The cloud droplet formation  
322 parameterization presented here has been extensively evaluated by comparing  
323 computations of  $N_d$  and  $s_{\max}$  and their sensitivity to aerosol properties against  
324 detailed numerical simulations of the activation process by a parcel-model  
325 (Betancourt and Nenes, 2014a).

326

### 327 2.3 Aerosol Precursor Emissions

328 Dust emission fluxes are calculated online by an advanced dust flux scheme  
329 developed by Astitha et al. (2012). This scheme uses an explicit geographical  
330 representation of the airborne soil particle size distribution based on soil  
331 characteristics in every grid cell. Emissions of crustal species ( $\text{Ca}^{2+}$ ,  $\text{Mg}^{2+}$ ,  $\text{K}^+$ ,  $\text{Na}^+$ )  
332 are estimated as a fraction of mineral dust emissions based on the chemical  
333 composition of the emitted soil particles in every grid cell (Karydis et al., 2016).

Field Code Changed

334 Emissions of sea spray aerosols are based on the offline monthly emission data set of  
335 AEROCOM (Dentener et al., 2006) assuming a composition of 55%  $\text{Cl}^-$ , 30.6%  $\text{Na}^+$ ,  
336 7.7%  $\text{SO}_4^{2-}$ , 3.7%  $\text{Mg}^{2+}$ , 1.2%  $\text{Ca}^{2+}$ , 1.1%  $\text{K}^+$  (Seinfeld and Pandis, 2006). The  
337 CMIP5 RCP4.5 emission inventory (Clarke et al., 2007) is used for the anthropogenic  
338 primary organic aerosol emissions from fossil fuel and biofuel combustion sources.  
339 The open biomass burning emissions from savanna and forest fires are based on the  
340 GFED v3.1 database (van der Werf et al., 2010). More details about the aerosol phase  
341 emissions used by EMAC can be found in Karydis et al. (2016) and Tsimpidi et al.  
342 (2016).

Field Code Changed

Field Code Changed

Field Code Changed

343 Related anthropogenic emissions of  $\text{NO}_x$ ,  $\text{NH}_3$ , and  $\text{SO}_2$ , which represent the  
344 gaseous precursors of the major inorganic components, are based on the monthly  
345 emission inventory of EDGAR-CIRCE (Doering, 2009) distributed vertically as  
346 presented in Pozzer et al. (2009). The natural emissions of  $\text{NH}_3$  are based on the  
347 GEIA database (Bouwman et al., 1997).  $\text{NO}_x$  produced by lightning is calculated  
348 online and distributed vertically based on the parameterization of Grewe et al. (2001).  
349 The emissions of  $\text{NO}$  from soils are calculated online based on the algorithm of  
350 Yienger and Levy (1995) as described in Ganzeveld et al. (2002). Eruptive and non-  
351 eruptive volcanic degassing emissions of  $\text{SO}_2$  are based on the AEROCOM data set  
352 (Dentener et al., 2006). The oceanic DMS emissions are calculated online by the

Field Code Changed

Field Code Changed

353 AIRSEA submodel (Pozzer et al., 2006). More details about the gas phase emissions  
354 used by EMAC can be found in Pozzer et al. (2012) and Karydis et al. (2016).

Field Code Changed

355

### 356 3. Model Results and Evaluation

357

#### 358 3.1 Model Predictions

359 The annual and seasonal (during DJF and JJA) mean CDNC<sub>2</sub> calculated by EMAC  
360 with UAF implementation for the lowest model level at which clouds are formed  
361 (centered at 940 ~~mb~~) ~~are shown in Figure 1. The~~hPa), ~~are shown in Figure 1. In this~~  
362 ~~study, CDNC is referred to the number concentration of droplets nucleated in-cloud~~  
363 ~~and represents an upper limit since droplet depletion by collision, coalescence and~~  
364 ~~collection are not taken into account. Therefore, the~~ calculated CDNC is mostly  
365 sensitive to the cloud updraft velocity and the total aerosol number concentration  
366 (Karydis et al., 2012), which are the main drivers of the  $s_{\max}$  calculations. The annual  
367 mean aerosol number concentration, updraft velocity, and  $s_{\max}$  ~~at 940 hPa, as well as~~  
368 ~~the low-level cloudiness~~ calculated by EMAC ~~at 940 mb~~ are shown in Figure 2. ~~The~~  
369 ~~calculated CDNC is also sensitive to the fraction of mineral dust present in the aerosol~~  
370 ~~since it can affect the aerosol-water vapor interactions by changing the exponent  $x$  in~~  
371 ~~Eq. 4. The annual mean insoluble fraction of the particles in the accumulation and~~  
372 ~~coarse mode (where mineral dust exists) are shown in figure 3.~~ The calculated global  
373 annual mean CDNC at 940 ~~mb~~hPa is  $231 \text{ cm}^{-3}$ .

Formatted: Space Before: 0 pt

374 Over the continents, the predicted annual mean CDNC is  $546 \text{ cm}^{-3}$  and exceeds  
375  $1000 \text{ cm}^{-3}$  over the industrialized areas of Europe, central and eastern Asia, and North  
376 America. In these areas, the aerosol number concentration is high (exceeding  $10,000$   
377  $\text{cm}^{-3}$ ; Figure 2a), while the calculated updraft velocities ( $0.5\text{-}1 \text{ m s}^{-1}$ ; Figure 2b) allow  
378 the development of sufficiently high  $s_{\max}$  ( $0.1\text{-}0.3\%$ ; Figure 2c) for the activation of  
379 5% (over eastern China) to 15% (over central Europe) of the pollution aerosols into  
380 cloud droplets. The simulated  $s_{\max}$  is close to the estimated  $s_{\max}$  ( $0.2\%\text{-}0.5\%$ ) for  
381 stratocumulus clouds based on data from continental air masses (Twomey and  
382 Wojciechowski, 1968; Martin et al., 1993) indicating that the combination of aerosol  
383 number concentration and updraft velocity in the model is realistic.

Field Code Changed

Field Code Changed

384 While the aerosol number concentration over the industrialized areas remains fairly  
385 constant throughout the year, the updraft velocity is higher during the boreal winter

386 (i.e., DJF) resulting in a seasonal peak of CDNC during DJF (exceeding  $2,000 \text{ cm}^{-3}$ )  
387 over North America, Europe and eastern Asia (Figure 1b). The highest annual mean  
388 CDNC is calculated over northern India ( $\sim 2,000 \text{ cm}^{-3}$ ) where the model simulates  
389 highest aerosol concentrations ( $\sim 30,000 \text{ cm}^{-3}$ ). Over Southeast Asia and India, CDNC  
390 peaks during JJA (exceeding  $2,000 \text{ cm}^{-3}$ ; Figure 1c), affected by the East Asian  
391 Monsoon and the high updraft velocities developed during the wet season. Relatively  
392 high CDNC (annual mean of  $300\text{-}700 \text{ cm}^{-3}$ ) are also calculated over the tropical  
393 regions of the Southern Hemisphere which are influenced by biomass burning.  
394 Relatively low values are calculated over the Congo Basin where the mean updraft  
395 velocity is typically low (below  $0.2 \text{ m s}^{-1}$ ) leading to low  $s_{\text{max}}$  (below 0.05%) and  
396 cloud droplet activation ( $\sim 300 \text{ cm}^{-3}$ ).

397 Downwind of deserts, the calculated CDNC varies between  $100 \text{ cm}^{-3}$  (e.g.,  
398 Patagonia, and Australian deserts) to  $1,000 \text{ cm}^{-3}$  (e.g., Sahara, Arabian, Taklimakan,  
399 Gobi and Atacama). In the vicinity of the Sahara and Arabian deserts, the mean  
400 updraft velocity is  $\sim 0.5 \text{ m s}^{-1}$ . However, downwind of the western part of the Sahara  
401 the aerosol number concentration is relatively low ( $\sim 1,000 \text{ cm}^{-3}$ ) leading to higher  
402  $s_{\text{max}}$  ( $\sim 0.2\%$ ) but low CDNC ( $\sim 200 \text{ cm}^{-3}$ ). On the other hand, downwind of the  
403 eastern Sahara and Arabian deserts the aerosol concentration is higher ( $2,000\text{-}3,000$   
404  $\text{cm}^{-3}$ ). Over these areas the presence of a high number of coarse dust particles  
405 significantly reduces  $s_{\text{max}}$  ( $\sim 0.05\%$ ), but at the same time they efficiently activate into  
406 cloud droplets (CDNC varies from  $500$  to  $1,000 \text{ cm}^{-3}$ ). Close to Patagonia and  
407 Australia, despite the high updraft velocities ( $\sim 1 \text{ m s}^{-1}$ ), the aerosol concentration is  
408 low (below  $500 \text{ cm}^{-3}$ ) and also CDNC is relatively low ( $\sim 100 \text{ cm}^{-3}$ ). The highest  
409 updraft velocities are calculated around the Atacama and Gobi deserts (over  $1 \text{ m s}^{-1}$ )  
410 leading to both high  $s_{\text{max}}$  (over 0.3%) and CDNC ( $\sim 1,000 \text{ cm}^{-3}$ ). However, the central  
411 Asian deserts (e.g., Gobi) are under the influence of the Siberian anticyclone during  
412 winter (i.e., DJF) which causes katabatic winds (that inhibit the formation of positive  
413 updraft velocities) and very low temperatures that prevent the formation of liquid  
414 [water](#) clouds.

415 Over the oceans, the predicted annual mean CDNC is  $113 \text{ cm}^{-3}$  and exceeds  $500$   
416  $\text{cm}^{-3}$  along the coasts of Mediterranean countries, China, India, SE Asia, California,  
417 the northeastern USA and western Africa (Fig. 1). Over many coastal regions aerosol  
418 concentrations are relatively high ( $5,000\text{-}10,000 \text{ cm}^{-3}$ ), however, the low updraft

419 velocities ( $\sim 0.2 \text{ m s}^{-1}$ ) result in lower CDNCs than over land (Figure 1). The  
420 Mediterranean and Yellow Seas are somewhat exceptional since the annual mean  
421 updraft velocities are higher in these regions ( $\sim 0.3 \text{ m s}^{-1}$ ), resulting in higher  $s_{\text{max}}$   
422 ( $\sim 0.1\%$  and  $\sim 0.3\%$ , respectively) and therefore high CDNC ( $\sim 800 \text{ cm}^{-3}$  and  
423  ~~$\sim 1200$~~   $1,200$   $\text{cm}^{-3}$ , respectively). The simulated  $s_{\text{max}}$  is in close agreement with  
424 estimates ( $\sim 0.1\%$ ) based on observational data over the eastern Mediterranean  
425 (Bougiatioti et al., 2016a; Kalkavouras et al., 2016). CDNC over these seas is subject  
426 to high seasonal variation ranging from  $\sim 400 \text{ cm}^{-3}$  ( $\sim 800 \text{ cm}^{-3}$ ) over the  
427 Mediterranean (Yellow) Sea during JJA, to over  $1,000 \text{ cm}^{-3}$  ( $2,000 \text{ cm}^{-3}$ ) during DJF  
428 due to the higher updraft velocities during boreal winter (exceeding  $1 \text{ m s}^{-1}$ ) compared  
429 to summer (below  $0.2 \text{ m s}^{-1}$ ). Over the northern coasts, the annual mean CDNC is  
430 significantly enhanced compared to the oceans of the Southern Hemisphere due to the  
431 transport of pollutants from industrialized areas in the Northern Hemisphere. Despite  
432 the high updraft velocities calculated over the southern oceans throughout the year (up  
433 to  $1 \text{ m s}^{-1}$ ), the lack of aerosol (typically below  $100 \text{ cm}^{-3}$ ) results in CDNC below  $50$   
434  $\text{cm}^{-3}$ . Finally, the calculated CDNC decreases with altitude due to the decrease in  
435 aerosol concentration by dilution and atmospheric removal (Figure 34). The global  
436 mean CDNC is predicted to be  $231 \text{ cm}^{-3}$ ,  $171 \text{ cm}^{-3}$ ,  $120 \text{ cm}^{-3}$ ,  $87 \text{ cm}^{-3}$ , and  $60 \text{ cm}^{-3}$  at  
437  ~~$940 \text{ mbhPa}$~~ ,  ~~$900 \text{ mbhPa}$~~ ,  ~~$860 \text{ mbhPa}$~~ ,  ~~$820 \text{ mbhPa}$~~ , and  ~~$770 \text{ mbhPa}$~~ , respectively.

438

### 439 3.2 Model Evaluation

440 The predicted in-cloud CDNC are compared to observational data from  
441 continental, polluted marine and clean marine regions around the world (Karydis et  
442 al., ~~2014~~ 2011a). The locations of observations (i.e., longitude, latitude, and altitude)  
443 and time of year have been taken into account in sampling the model results. Given  
444 that the observations span a decade, in contrast to the simulation which represents one  
445 year, the month of each campaign has been used to account for the seasonal  
446 variability of the CDNC. Thus, the implicit assumption is that inter-annual variability  
447 can be neglected. It should also be mentioned that the observations typically do not  
448 represent monthly means over  $1.9^\circ$  grid squares, as sampled from the model results,  
449 so that the comparison is more qualitative than quantitative. ~~A summary of the~~  
450 ~~comparison results is presented in Table 1 and Figure 4. Furthermore, the cloud-~~  
451 ~~averaged CDNC for stratocumulus clouds, which are described by EMAC, is typically~~

Field Code Changed

452 well captured by the cloud droplet formation parameterization used in this study  
453 (Meskhidze et al., 2005; Fountoukis et al., 2007; Morales et al., 2011), while the  
454 droplet collision and coalescence processes, which are neglected here, are becoming  
455 important only in the presence of clouds with substantial amount of drizzle. A  
456 summary of the comparison results is presented in Table 1 and Figure 5. The mean  
457 bias (MB), mean absolute gross error (MAGE), normalized mean bias (NMB),  
458 normalized mean error (NME), and the root mean square error (RMSE) are used to  
459 assess the model performance (Table 2).

460 The model captures the low values (below  $100 \text{ cm}^{-3}$ ) observed over the remote  
461 Pacific, Atlantic and Indian Oceans and at the same time is capable of simulating the  
462 higher concentrations ( $>100 \text{ cm}^{-3}$ ) observed over the eastern Pacific Ocean (Table 1).  
463 On the other hand, it falls short in reproducing the relatively high CDNC ( $>100 \text{ cm}^{-3}$ )  
464 observed during summer over the western Arctic Ocean and over the remote area west  
465 of Australia. Overall, the model tends to underestimate the CDNC over remote oceans  
466 with a MB =  $-33 \text{ cm}^{-3}$  and NMB = -39% (Table 2).

467 Both the observed and simulated CDNC show significant increases over polluted  
468 marine regions close to the coasts (Table 1; Figure 4a5a). Compared to satellite  
469 retrievals (Bennartz, 2007; Rausch et al., 2010), the model reproduces the CDNC over  
470 the American and African coasts well, but it significantly overestimates CDNC along  
471 the Asian coasts (Table 1). Compared to in situ observations, the model reproduces  
472 the high CDNC along coastal areas in the Northern Hemisphere (e.g., the Yellow Sea,  
473 Oregon, Florida, Canary Islands), but systematically overestimates CDNC over the  
474 British coasts. Further, the model does not reproduce some of the high CDNC  
475 observations over more remote areas (i.e., over the Azores and eastern Atlantic  
476 Ocean). Overall, the model tends to overestimate the CDNC over polluted marine  
477 areas with a MB =  $127 \text{ cm}^{-3}$  and NMB = 75% (Table 2).

478 The observed CDNC over continental regions is subject to high spatial variability,  
479 with reported values ranging from  $<100 \text{ cm}^{-3}$  over Alaska (Dong and Mace, 2003) to  
480  $>1,000 \text{ cm}^{-3}$  over China (Zhao et al., 2006), England (Bower et al., 1999), and the  
481 continental USA (Fountoukis et al., 2007). The model captures the observed  
482 variability with low values over remote areas (e.g., over Alaska) and high values over  
483 the industrialized parts of the Northern Hemisphere (i.e., East Asia, Europe, and  
484 China). Overall, the model overestimates CDNC over most continental regions (MB=  
485  $269 \text{ cm}^{-3}$  and NMB=58%; Table 2). Over China, the simulated CDNC is within the

Field Code Changed

Field Code Changed

486 observed range with the exception of Hebei Province where it significantly  
487 overestimates measured CDNC (Table 1). In Europe, the model reproduces the high  
488 CDNC observed over Central Europe and England but it clearly overestimates the low  
489 CDNC values observed over Finland. Over North America, the model captures the  
490 variability of the observed CDNC, predicting lower values over remote areas (e.g.,  
491 Alaska) and higher values over the industrialized areas of USA (e.g., Ohio and  
492 Michigan). It tends to overestimate the CDNC over the continental USA and  
493 underestimate the observed values over Alaska.

494 ~~Over all examined regions (clean marine, polluted marine, continental). Globally,~~  
495 the calculated NMB is 56% and the NME is 82%, indicating that some of the  
496 discrepancy between the modelled and the observed CDNC is explained by  
497 uncertainties in the observations and the numerical simulations. Around 60% of the  
498 simulated CDNC are within a factor of 2 compared to the measurements (Figure  
499 ~~4a5a~~) and 40% of the simulated CDNC differ less than 30% from the measurements.  
500 Based on the typical properties of marine stratus clouds, a uniform increase in global  
501 CDNC by 30% (or 50%) ~~can result in~~ leads to an increase in cloud albedo of 2.25%  
502 (or 3.75%) and a perturbation of  $-1.1 \text{ W m}^{-2}$  (or  $-1.7 \text{ W m}^{-2}$ ) in the global mean cloud  
503 radiative forcing (Schwartz, 1996). However, the simulated CDNC presented here  
504 refers to the number concentration of droplets nucleated in clouds and represents an  
505 upper limit with respect to the comparison with observations, since collision and  
506 coalescence processes, which are not taken into account here, can reduce the CDNC.

Field Code Changed

507

#### 508 4. Mineral Dust Effect on CDNC

509

##### 510 4.1 Total Impact of Mineral Dust on CDNC

511 To estimate the overall effect of mineral dust on CDNC a sensitivity run was  
512 conducted switching off the mineral dust emissions. Figure ~~56~~ depicts the difference  
513 in CDNC between the base case simulation and the sensitivity test. A positive change  
514 corresponds to an increase of the CDNC due to the presence of dust. The predicted  
515 CDNC is typically increased by the presence of dust aerosols over the main deserts  
516 (Figure ~~56~~). Over the Sahara, CDNC increases less than  $50 \text{ cm}^{-3}$  (up to 20%). The  
517 largest change is calculated downwind of the Patagonian ( $\sim 150 \text{ cm}^{-3}$  or 70%) and  
518 Atacama ( $\sim 350 \text{ cm}^{-3}$  or 40%) deserts. Over these deserts dust emissions increase the  
519 aerosol concentration by more than  $5,000 \text{ cm}^{-3}$  (Figure 6c). The effect of mineral dust

520 on CDNC close to Sahara varies significantly throughout the year due to the  
521 seasonality of the mineral dust emissions. Over the sub-Saharan region, CDNC  
522 increases by up to  $150 \text{ cm}^{-3}$  during DJF, owing to the northeasterly trade winds (i.e.,  
523 Harmattan winds) which blow from the Sahara Desert over ~~the~~ West Africa during  
524 winter. Over the eastern Sahara and the Arabian deserts CDNC ~~increase~~ increases up  
525 to  $150 \text{ cm}^{-3}$  during spring (i.e., MAM) and autumn (i.e., SON) when the Sirocco  
526 winds are most common.

527 In contrast to regions close to deserts, CDNC decreases over the polluted regions  
528 of the Northern Hemisphere and especially over southern Europe ( $\sim 100$  or less than  
529 10%) and northeastern Asia (up to  $400 \text{ cm}^{-3}$  or 20%). In these areas, dust particles  
530 transported from the Sahara over Europe and from the Gobi and Taklimakan deserts  
531 over Asia, are mixed with anthropogenic particles decreasing the total aerosol number  
532 concentration (Figure 6c), due to coagulation, and affecting the aerosol-water vapor  
533 interactions.

534 As the insoluble fraction of aerosols increases, due to the addition of mineral dust  
535 (Figures 3b and 3c), the exponent  $x$  in Eq. 4 changes, resulting in a decrease of the  
536 number of activated droplets. Furthermore, the relatively large, aged dust particles  
537 over these areas activate early on in the cloud formation process, taking up much  
538 water per particle and thus reducing  $s_{\text{max}}$  ( $\sim 15\%$ ), and consequently cloud droplet  
539 formation on the smaller anthropogenic particles (e.g., the activated fraction of the  
540 particles in the accumulation mode reduces by 20%). Beside microphysical effects,  
541 the presence of mineral dust can also affect cloud formation by altering the energy  
542 balance of the atmosphere, and thus turbulent motions and the updraft velocity.

543 Nevertheless, the calculated updraft velocity does not change significantly between  
544 the two simulations (less than 5% ~~since~~), in part because the meteorology is  
545 dynamically nudged to analysis data (Jeuken et al., 1996). CDNC also decreases over  
546 the oceans downwind of deserts in the Northern Hemisphere, and even over the  
547 rainforests in the Southern Hemisphere ( $\sim 150$  or 30%). ~~Overall, despite~~ Overall, the  
548 impact of mineral dust on CDNC is positive only in areas with low cloud cover (i.e.,  
549 over the main deserts where cloud cover is typically lower than 5%; Figure 2d). On  
550 the other hand, mineral dust negatively affects cloud droplet formation over areas  
551 with high cloud cover (e.g., over Europe and Eastern Asia). Despite that CDNC  
552 increases over the deserts due to the presence of dust particles, the decrease of CDNC

553 over the industrialized and forested continental areas dominates the calculated global  
554 average change, i.e., the calculated global average CDNC decreases by 11% (or 26  
555  $\text{cm}^{-3}$ ).

556

#### 557 4.2 Impact of Mineral Dust Chemistry on CDNC

558 To estimate the effects of thermodynamic mineral dust interactions with inorganic  
559 anions on the predicted CDNC, a sensitivity run was conducted by switching off the  
560 dust-aerosol chemistry. ~~Karydis et al. (2016)~~ have shown that dust can significantly  
561 affect the partitioning of inorganic aerosol components and especially nitrate.

562 Analogous to ~~(Karydis et al. (2016))~~; Karydis et al. (2016), accounting for  
563 thermodynamic interactions of mineral dust in our simulations results in an increase  
564 of the tropospheric burden of nitrate, chloride, and sulfate aerosols by 44%, 9%, and  
565 7%, respectively. On the other hand, ammonium decreases by 41%. The dust presence  
566 itself also decreases by 14% since it becomes significantly more soluble, mostly due  
567 to the condensation of nitric acid on its surface, and is removed more efficiently  
568 through wet and dry deposition, the latter partially due to the increased sedimentation  
569 by dust particles that have a larger water content. Therefore, the calculated change of  
570 CDNC (Figures ~~6a7a~~ and ~~6b7b~~) is the net result of counterbalancing effects. Due to  
571 the increase of the soluble fraction by considering mineral dust chemistry, the CDNC  
572 activated from dust particles increases (Figure ~~6e7c~~), while the total number of dust  
573 particles and the CDNC from insoluble particles decreases (Figure ~~6d7d~~). Taking as  
574 an example a grid cell over the Sahara ~~desert~~Desert, the model simulations indicate  
575 that by switching on~~accounting for~~ the mineral dust chemistry, the soluble fraction of  
576 the dust containing particles increases by 0.07, resulting in an increase of CDNC  
577 activated from soluble aerosol modes by  $150 \text{ cm}^{-3}$  (Figure ~~6e7c~~). On the other hand,  
578 the aerosol number concentration decreases by  $90 \text{ cm}^{-3}$  due to the more efficient  
579 atmospheric removal of the aged dust particles, resulting in a decrease of the CDNC  
580 activated from the insoluble modes by  $50 \text{ cm}^{-3}$  (Figure ~~6d7d~~). The net effect is that the  
581 total CDNC increases by  $100 \text{ cm}^{-3}$  (Figure ~~6a7a~~).

582 Overall, the presence of reactive dust components results in an increase of CDNC  
583 over the deserts that are close to anthropogenic sources, e.g., up to  $100 \text{ cm}^{-3}$  (or 20%)  
584 over the Sahara and up to  $200 \text{ cm}^{-3}$  (or 30%) over the Arabian Peninsula. In these  
585 areas, the CCN activity of mineral dust (initially hydrophilic) is enhanced by the  
586 acquired hygroscopicity from the anthropogenic (including biomass burning) aerosol

Field Code Changed

587 | compounds (mainly nitrate) ~~during their thermodynamic interaction.~~ Even though  
588 | the chemically aged dust particles activate into droplets more efficiently than  
589 | insoluble ones, their reduced number concentration dominates the calculated effect on  
590 | CDNC over the relatively pristine remote desert regions, e.g., CDNC decreases up to  
591 |  $200 \text{ cm}^{-3}$  (or 20%) downwind of the Taklimakan,  $250 \text{ cm}^{-3}$  (or 30%) around the  
592 | Atacama, and up to  $100 \text{ cm}^{-3}$  (or 40%) over the Patagonian deserts. Even over the  
593 | rainforests,  $\text{HNO}_3$  from  $\text{NO}_x$ , emitted by biomass burning  ~~$\text{NO}_x$~~  thermodynamically  
594 | interacts with the coarse soil particles from the upwind deserts, resulting in an  
595 | increase of CDNC by around  $50 \text{ cm}^{-3}$ . CDNC is also slightly increased over Europe  
596 | and eastern Asia (up to  $150 \text{ cm}^{-3}$  or about 10%) where  $\text{HNO}_3$  from anthropogenic  
597 |  $\text{NO}_x$  sources interacts with mineral dust from the surrounding deserts. While the  
598 | global average CDNC does not change much by taking into account thermodynamic  
599 | and chemical interactions of mineral dust with inorganic air pollutants, CDNC spatial  
600 | distributions change substantially.

601

#### 602 | **4.3 Impact of Water Adsorption by Mineral Dust on CDNC**

603 | To estimate the effects of water adsorption onto the surface of insoluble dust  
604 | particles on CDNC, a sensitivity run was conducted by switching off the FHH  
605 | adsorption calculations. In this sensitivity simulation, the soluble modes follow the  $\kappa$ -  
606 | Köhler theory while insoluble modes do not participate in cloud droplet formation  
607 | calculations. Figure 78 depicts the difference in CDNC between the base case  
608 | simulation and this sensitivity test. A positive change corresponds to an increase of  
609 | the CDNC from water adsorption on mineral dust. The calculations show that CDNC  
610 | is increased by applying FHH theory over several arid areas where the insoluble dust  
611 | concentration is high (Figure 78), since  $\kappa$ -Köhler theory does not take into account the  
612 | contribution of insoluble particles to cloud droplet formation. CDNC is increased in  
613 | the vicinity of the ~~Sahara~~Saharan, Arabian and Thar deserts ( $\sim 100 \text{ cm}^{-3}$  or about  
614 |  $\pm 20\%$ ) where the insoluble fraction of mineral dust is larger due to the small  
615 | anthropogenic emission influence that makes the particles hygroscopic. On the other  
616 | hand, CDNC decreases over the polluted regions of the Northern Hemisphere and  
617 | especially over Europe ( $\sim 100 \text{ cm}^{-3}$  or about  $\pm 10\%$ ) and Asia (up to  $\sim 400 \text{ cm}^{-3}$  or  $\pm$   
618 | 20%). Over these areas, the added hydrophilicity by the soluble coatings on the  
619 | surface of the aged dust particles increases their water uptake during activation.  
620 | Therefore, the aged dust particles relatively strongly compete for water vapor,

621 reducing the  $s_{\max}$  (~15%) and thus cloud droplet formation from the smaller  
622 anthropogenic particles. Over the tropical rainforests CDNC decreases by  
623 ~~approximately ~150 cm<sup>-3</sup> (or about ~30%)~~. Overall, the use of the UAF results in a  
624 decrease of the global average CDNC by ~10% (or about ~~~23 cm<sup>-3</sup>~~).

625

## 626 5 Additional Sensitivity Tests

627 Three additional sensitivity simulations were conducted to investigate the CDNC  
628 dependency on i) the chemical composition of the emitted dust aerosols, ii) the  
629 hydrophilicity of mineral dust, and iii) the strength of the dust aerosol emissions.  
630 Figure 89 depicts the absolute annual mean changes in CDNC compared to the  
631 reference simulation for each of the sensitivity tests. A positive change corresponds to  
632 an increase of the CDNC relative to the reference.

633

### 634 5.1 Sensitivity to the emitted dust aerosol composition

635 The first sensitivity test assumes a globally uniform chemical composition of  
636 mineral dust (Sposito, 1989), in contrast to the reference simulation where the mineral  
637 dust composition depends on the soil characteristics of each desert (Karydis et al.,  
638 2016). While the emitted mineral dust load remains the same in the sensitivity  
639 simulation, the different mineral dust composition results in significant changes in the  
640 calculated tropospheric burdens of dust components (Karydis et al., 2016). In  
641 particular, the fraction of the mineral components relative to the total dust in the  
642 sensitivity simulation is lower over most of the deserts compared to the reference.  
643 This reduction of the chemically reactive mineral components in the sensitivity  
644 simulation results in a slowdown of the mineral dust aging and hence in an increase of  
645 its concentration due to the reduced atmospheric removal. Conversely, the CCN  
646 activity of dust particles is higher in the reference simulation since the chemical aging  
647 is ~~stronger~~ more efficient compared to the sensitivity simulation. These  
648 counterbalancing effects result in negligible changes of CDNC worldwide (less than  
649 10%).

650

651

652

### 653 5.2 Sensitivity to the hydrophilicity of dust

Field Code Changed

654 The second sensitivity test assumes increased hydrophilicity of mineral dust  
655 aerosols by using a 10% lower  $B_{FHH}$  parameter ( $B_{FHH}=1.1$ ). The  $B_{FHH}$  parameter  
656 directly affects the CCN activity of dust particles by changing the equilibrium  
657 supersaturation (Eq. 3) and the “CCN spectrum” (Eq. 4) through the exponent  $x$ .  
658 Kumar et al. (2011b) tested the CCN activity of aerosols dry generated from clays,  
659 calcite, quartz, and desert soil samples from Northern Africa, East Asia/China, and  
660 Northern America. They found that  $B_{FHH}$ , which strongly affects the equilibrium  
661 curve, varied from 1.12 to 1.30 (i.e.,  $\pm 10\%$  from 1.2 which is the value used in our  
662 base case simulation). Therefore, the sensitivity test presented here can represent the  
663 potential impacts on the results due the simplification of using a globally uniform set  
664 of FHH parameters to describe the hydrophilicity of mineral dust independently of its  
665 source and composition. The higher hydrophilicity of mineral dust in the sensitivity  
666 simulation results in increased CDNC over ~~over~~ areas close to deserts by up to 30%  
667 (e.g.,  $100\text{ cm}^{-3}$  over Sahara and  $200\text{ cm}^{-3}$  over Gobi and Taklimakan). A notable  
668 increase is also calculated over eastern China and northern India (up to  $150\text{ cm}^{-3}$  or  
669 10%) where mineral dust is mixed with anthropogenic compounds. These results  
670 indicate that changes in the hydrophilicity of the freshly emitted dust, due to the  
671 variability of its composition with source region, can have an important impact on the  
672 calculated CDNC. Remote from the main deserts (e.g., over central Europe), the  
673 change in CDNC is negligible since the contribution of mineral dust particles on  
674 cloud droplet formation is low. Overall, the calculated global average CDNC  
675 increases in the sensitivity simulation by about 5% (or  $\sim 12\text{ cm}^{-3}$ ).

676

### 677 **5.3 Sensitivity to the emitted dust aerosol load**

678 The final sensitivity test assumes 50% lower emissions of mineral dust compared  
679 to the reference simulation. The lower tropospheric dust-~~aerosol~~ load in the sensitivity  
680 simulation (49%) results in a 10-30% (up to  $150\text{ cm}^{-3}$ ) decrease of CDNC over the  
681 main deserts. On the other hand, CDNC increases over the anthropogenic (e.g., East  
682 Asia) and biomass burning (e.g., central Africa) regions by 5-10% (up to  $150\text{ cm}^{-3}$ ).  
683 The opposing responses of CDNC to mineral dust emissions result from the fact that  
684 the tropospheric load of the other aerosol species does not change significantly  
685 between the two simulations since the chemical and thermodynamic interactions of  
686 mineral cations with air pollution ~~are still important~~ remain predominant, even after

687 | the 50% dust emission reduction, i.e., the nitrate abundance rather than that of dust is  
688 | rate limiting. Therefore, the presence of inorganic anions (e.g.,  $\text{NO}_3^-$ ) in the aerosol  
689 | phase remains almost unchanged between the two simulations, which results in a  
690 | decrease of the insoluble fraction of the aerosol, given that mineral dust  
691 | concentrations are significantly lower in the reference simulation, leading to higher  
692 | CCN activity. Over the Taklimakan desert the insoluble fraction of the aerosol  
693 | changes by less than 10%, and therefore, the change in aerosol number concentration  
694 | (~40%) due to the mineral dust emission change dominates the effect on CDNC,  
695 | which is calculated to be about  $100 \text{ cm}^{-3}$  (or ~20%) lower in the sensitivity  
696 | simulation. On the other hand, over Southeast Asia, the aerosol number concentration  
697 | changes less than 10% whileas the insoluble fraction of the aerosols decreases by  
698 | 40%. The significant decrease of  $\varepsilon_i$  in Eq. (3) affects the calculated critical  
699 | supersaturation of the particle as well as the exponent  $x$  in Eq. (4) resulting in an  
700 | increase of CDNC by about  $150 \text{ cm}^{-3}$  (or ~10%). Overall, the impact of halving  
701 | mineral dust emissions on the calculated global average CDNC is remarkably small  
702 | (~3% or  $6 \text{ cm}^{-3}$ ).

703 |  
704 |

## 705 | **6 Summary and Conclusions**

706 | This study assesses the impact of mineral dust on global cloud droplet number  
707 | concentrations by using an interactive aerosol-chemistry-cloud-climate model  
708 | (EMAC). The “unified dust activation framework” (UAF) has been implemented into  
709 | the EMAC model to account for the effects of dust particles through both the  
710 | hydrophilicity from adsorption and the acquired hygroscopicity from pollution solutes  
711 | (chemical aging) on CCN activity calculations. The calculation of cloud droplet  
712 | formation from soluble particles is carried out by using the  $\kappa$ -Köhler theory, while  
713 | that of insoluble particles is based on the FHH multilayer adsorption isotherm  
714 | approach. For atmospheric particles that contain a substantial fraction of both soluble  
715 | (e.g., nitrate) and insoluble material (e.g., mineral dust), cloud formation is calculated  
716 | using the UAF, which determines the maximum equilibrium water vapor  
717 | supersaturation over an aerosol consisting of an insoluble core with a soluble coating.  
718 | Furthermore, the model setup includes thermodynamic interactions between mineral  
719 | dust anions (i.e.,  $\text{Na}^+$ ,  $\text{Ca}^{2+}$ ,  $\text{K}^+$ ,  $\text{Mg}^{2+}$ ) and inorganic cations (i.e.,  $\text{NO}_3^-$ ,  $\text{Cl}^-$ ,  $\text{SO}_4^{2-}$ ).

720 The simulated CDNC at 940 ~~mbhPa~~, i.e., at cloud base, is relatively high over the  
721 industrialized areas of Europe, Asia and North America (exceeding  $1,000 \text{ cm}^{-3}$ ) and  
722 over the biomass burning regions in the tropics ( $300\text{-}700 \text{ cm}^{-3}$ ). Relatively high  
723 CDNC is also calculated over the main deserts ( $100\text{-}1,000 \text{ cm}^{-3}$ ) where the CCN  
724 activity of pristine mineral dust is enhanced by chemical and thermodynamic  
725 interactions with soluble compounds from anthropogenic (including biomass burning)  
726 and natural sources. Low CDNC (around  $50 \text{ cm}^{-3}$ ) is calculated over the remote  
727 oceans while CDNC is much higher (up to  $1,000 \text{ cm}^{-3}$ ) over more polluted marine  
728 regions near the coast. In view of CDNCs from in situ and satellite observations, we  
729 conclude that the model tends to underestimate CDNC over clean marine areas and  
730 overestimates CDNC over polluted regions. In the current application, CDNC  
731 represents an upper limit with respect to the comparison with observations since we  
732 have not accounted for droplet depletion through collision and coalescence processes.  
733 However, the model tendency to overestimate the high values of CDNC has small  
734 impact on the overall cloud radiative forcing since the sensitivity of cloud albedo to  
735 CDNC over polluted areas is low (Seinfeld and Pandis, 2006).

736 To estimate the effects of mineral dust and its variable chemical composition on  
737 CDNC, three main sensitivity simulations have been conducted. In the first, mineral  
738 dust emissions were switched off. This reveals that despite the large tropospheric load  
739 of mineral dust aerosols (35 Tg in the base case simulation) the dust presence  
740 decreases the calculated global average CDNC by only 11%. This is the net result of  
741 substantial positive and negative, partly compensating effects. Over polluted regions  
742 (e.g., Europe), dust particles, mostly transported from the Sahara, are mixed with  
743 pollution aerosols resulting in a significant reduction of the CCN activity of the  
744 anthropogenic particles and hence cloud droplet formation. On the other hand, the  
745 activation of freshly emitted dust particles through water adsorption results in an  
746 increase of CDNC over the main deserts. However, on a global scale this ~~does~~  
747 ~~not~~ match equivalent with the calculated decrease over the polluted regions. While such  
748 sensitivity tests do not relate to real-world changes, they help understand the role of  
749 mineral dust in the climate system, and especially the importance of including these  
750 processes into climate models, being hitherto neglected.

751 A second simulation has been performed by switching off the mineral dust  
752 chemistry to estimate the impact of interactions between inorganic and mineral  
753 cations on the predicted CDNC. We find that the tropospheric burden of inorganic

754 anions (mainly nitrate) increases, resulting in a slight increase of CCN activity and  
755 cloud droplet formation efficiency in areas that are influenced by biomass burning and  
756 industrial emissions. Furthermore, including crustal cation chemistry and  
757 thermodynamics significantly affects the aging of mineral dust and its solubility,  
758 especially due to the uptake of nitric acid, so that dust is removed more efficiently  
759 through wet and dry deposition. This results in a decrease of CDNC over the remote  
760 deserts (e.g., Taklimakan). ~~On average, global~~ Irrespective of the regional differences,  
761 the global average CDNC does not change significantly by considering mineral dust  
762 chemistry and thermodynamics.

763 In the third simulation, the FHH calculations have been switched off to estimate  
764 the effects of water adsorption onto the surface of insoluble dust particles on the  
765 predicted CDNC. The CDNC in the reference simulation is found to be higher over  
766 arid areas due to the adsorption activation of the freshly emitted insoluble dust  
767 particles. On the other hand, CDNC is lower over polluted regions (e.g., over Europe)  
768 since the aged dust particles experience significant water uptake during their  
769 activation reducing the  $s_{\max}$  and the activation of the smaller anthropogenic particles.  
770 Overall, the use of the UAF results in a decrease of the global average CDNC by  
771 ~10%. This result shows that for the modeling of cloud droplet formation, adsorption  
772 activation of insoluble aerosols ~~is~~ can be more important than mineral dust chemistry  
773 and thermodynamics. However, taking into account the adsorption activation of  
774 insoluble aerosols without mineral dust chemistry can result in a significant  
775 overestimation of CDNC, mainly over the remote deserts. Conversely, considering  
776 mineral dust chemistry and thermodynamics without UAF can result in significant  
777 overestimation of CDNC over polluted areas.

778 Finally, three additional sensitivity simulations have been conducted to investigate  
779 the sensitivity of the results to the physicochemical properties of the emitted mineral  
780 dust (chemical composition, hydrophilicity and emission strength). ~~This indicates~~ The  
781 results indicate that the calculated CDNC ~~is~~ can be regionally sensitive to the mineral  
782 dust hydrophilicity and emission load. ~~By~~ Nevertheless, by assuming drastic  
783 differences in the dust source and the dust hydrophilicity, we find only small (~5%)  
784 changes in the ~~average CDNC. Further,~~ global average CDNC. Larger CDNC changes  
785 are calculated over the main deserts (up to 30%) and over highly polluted areas (up to

786 | 10%). Further, we find that the global average CDNC is not sensitive to the chemical  
787 composition of mineral dust.

788 This study demonstrates that a comprehensive treatment of the CCN activity of  
789 mineral dust aerosols and their chemical and thermodynamic interactions with  
790 inorganic species by CCMs is important to realistically account for aerosol-chemistry-  
791 cloud-climate interactions. Neglecting the adsorption activation of freshly emitted  
792 dust can result in significant biases over areas close to deserts. In addition, neglecting  
793 the mineral dust chemistry and thermodynamics results in an underestimation of the  
794 coating of dust by hygroscopic salts during atmospheric aging. The realistic  
795 representation of soluble coating on dust is crucial since it affects its efficiency to  
796 grow by water uptake, which significantly influences the local supersaturation and  
797 thus cloud droplet formation over anthropogenically polluted regions. In this first  
798 study we apply the UAF diagnostically, while ~~for~~in future applications, e.g., to  
799 simulate climate ~~effects~~responses, we plan prognostic-~~climate~~ calculations where  
800 effects on precipitation formation and dynamical responses will also be accounted for.

801

## 802 **Acknowledgements**

803 V.A. Karydis acknowledges support from a FP7 Marie Curie Career Integration  
804 Grant (project reference 618349). A.P. Tsimpidi acknowledges support from a DFG  
805 individual ~~grant~~grandgrant program (project reference TS 335/2-1).

806

807

808 **References**

809

- 810 Abdelkader, M., Metzger, S., Mamouri, R. E., Astitha, M., Barrie, L., Levin, Z., and  
811 Lelieveld, J.: Dust-air pollution dynamics over the eastern Mediterranean,  
812 *Atmospheric Chemistry and Physics*, 15, 9173-9189, 2015.
- 813 Albrecht, B. A.: Aerosols, cloud microphysics, and fractional cloudiness, *Science*,  
814 245, 1227-1230, 1989.
- 815 Andreae, M. O. and Rosenfeld, D.: Aerosol-cloud-precipitation interactions. Part 1.  
816 The nature and sources of cloud-active aerosols, *Earth-Science Reviews*, 89, 13-  
817 41, 2008.
- 818 Astitha, M., Lelieveld, J., Kader, M. A., Pozzer, A., and de Meij, A.: Parameterization  
819 of dust emissions in the global atmospheric chemistry-climate model EMAC:  
820 impact of nudging and soil properties, *Atmospheric Chemistry and Physics*, 12,  
821 11057-11083, 2012.
- 822 Bangert, M., Nenes, A., Vogel, B., Vogel, H., Barahona, D., Karydis, V. A., Kumar,  
823 P., Kottmeier, C., and Blahak, U.: Saharan dust event impacts on cloud formation  
824 and radiation over Western Europe, *Atmospheric Chemistry and Physics*, 12, 4045-  
825 4063, 2012.
- 826 Barahona, D. and Nenes, A.: Parameterization of cloud droplet formation in large-  
827 scale models: Including effects of entrainment, *J. Geophys. Res.*, 112,  
828 doi:10.1029/2007JD008473 2007.
- 829 Barahona, D., West, R. E. L., Stier, P., Romakkaniemi, S., Kokkola, H., and Nenes,  
830 A.: Comprehensively accounting for the effect of giant CCN in cloud activation  
831 parameterizations, *Atmos. Chem. Phys.*, 10, 2467-2473, 2010.
- 832 Begue, N., Tulet, P., Pelon, J., Aouizerats, B., Berger, A., and Schwarzenboeck, A.:  
833 Aerosol processing and CCN formation of an intense Saharan dust plume during  
834 the EUCAARI 2008 campaign, *Atmospheric Chemistry and Physics*, 15, 3497-  
835 3516, 2015.
- 836 Bennartz, R.: Global assessment of marine boundary layer cloud droplet number  
837 concentration from satellite, *J. Geophys. Res.*, 112, doi: 10.1029/2006JD007547  
838 2007.
- 839 Betancourt, R. M. and Nenes, A.: Droplet activation parameterization: the population-  
840 splitting concept revisited, *Geoscientific Model Development*, 7, 2345-2357,  
841 2014a.
- 842 Betancourt, R. M. and Nenes, A.: Understanding the contributions of aerosol  
843 properties and parameterization discrepancies to droplet number variability in a  
844 global climate model, *Atmospheric Chemistry and Physics*, 14, 4809-4826, 2014b.
- 845 Bougiatioti, A., Bezantakos, S., Stavroulas, I., Kalivitis, N., Kokkalis, P., Biskos, G.,  
846 Mihalopoulos, N., Papayannis, A., and Nenes, A.: Biomass-burning impact on  
847 CCN number, hygroscopicity and cloud formation during summertime in the  
848 eastern Mediterranean, *Atmospheric Chemistry and Physics*, 16, 7389-7409,  
849 2016a.
- 850 Bougiatioti, A., Nikolaou, P., Stavroulas, I., Kouvarakis, G., Weber, R., Nenes, A.,  
851 Kanakidou, M., and Mihalopoulos, N.: Particle water and pH in the eastern  
852 Mediterranean: source variability and implications for nutrient availability,  
853 *Atmospheric Chemistry and Physics*, 16, 4579-4591, 2016b.
- 854 Bouwman, A. F., Lee, D. S., Asman, W. A. H., Dentener, F. J., VanderHoek, K. W.,  
855 and Olivier, J. G. J.: A global high-resolution emission inventory for ammonia,  
856 *Global Biogeochemical Cycles*, 11, 561-587, 1997.

Formatted: Font: 12 pt

857 Bower, K. N., Choulaton, T. W., Gallagher, M. W., Colvile, R. N., Beswick, K. M.,  
858 Inglis, D. W. F., Bradbury, C., Martinsson, B. G., Swietlicki, E., Berg, O. H.,  
859 Cederfelt, S. I., Frank, G., Zhou, J., Cape, J. N., Sutton, M. A., McFadyen, G. G.,  
860 Milford, C., Birmili, W., Yuskiewicz, B. A., Wiedensohler, A., Stratmann, F.,  
861 Wendisch, M., Berner, A., Ctyroky, P., Galambos, Z., Mesfin, S. H., Dusek, U.,  
862 Dore, C. J., Lee, D. S., Pepler, S. A., Bizjak, M., and Divjak, B.: The Great Dun  
863 Fell Experiment 1995: an overview, *Atmospheric Research*, 50, 151-184, 1999.

864 Capps, S. L., Henze, D. K., Hakami, A., Russell, A. G., and Nenes, A.:  
865 ANISORROPIA: the adjoint of the aerosol thermodynamic model ISORROPIA,  
866 *Atmospheric Chemistry and Physics*, 12, 527-543, 2012.

867 Clarke, L., Edmonds, J., Jacoby, H., Pitcher, H., Reilly, J., and Richels, R.: Scenarios  
868 of greenhouse gas emissions and atmospheric concentrations (Part A) and review  
869 of integrated scenario development and application (Part B). A report by the U.S.  
870 climate change science program and the subcommittee on global change research,  
871 2007. 2007.

872 Considine, D. B., Bergmann, D. J., and Liu, H.: Sensitivity of Global Modeling  
873 Initiative chemistry and transport model simulations of radon-222 and lead-210 to  
874 input meteorological data, *Atmospheric Chemistry and Physics*, 5, 3389-3406,  
875 2005.

876 Dall'Osto, M., Harrison, R. M., Highwood, E. J., O'Dowd, C., Ceburnis, D., Querol,  
877 X., and Achterberg, E. P.: Variation of the mixing state of Saharan dust particles  
878 with atmospheric transport, *Atmospheric Environment*, 44, 3135-3146, 2010.

879 de Meij, A., Pozzer, A., Pringle, K. J., Tost, H., and Lelieveld, J.: EMAC model  
880 evaluation and analysis of atmospheric aerosol properties and distribution with a  
881 focus on the Mediterranean region, *Atmos. Res.*, 114, 38-69, 2012.

882 Dentener, F., Kinne, S., Bond, T., Boucher, O., Cofala, J., Generoso, S., Ginoux, P.,  
883 Gong, S., Hoelzemann, J. J., Ito, A., Marelli, L., Penner, J. E., Putaud, J. P., Textor,  
884 C., Schulz, M., van der Werf, G. R., and Wilson, J.: Emissions of primary aerosol  
885 and precursor gases in the years 2000 and 1750 prescribed data-sets for AeroCom,  
886 *Atmos. Chem. Phys.*, 6, 4321-4344, 2006.

887 Doering, U., van Aardenne, J., Monni, S., Pagliari, V., Orlandini, L., and SanMartin,  
888 F.: CIRCE report D8.1.3 – Update of gridded emission inventories, addition of  
889 period 1990–2005 and the years 2010, 2015, 2050, 036961, 2009.

890 Dong, X. Q. and Mace, G. G.: Arctic stratus cloud properties and radiative forcing  
891 derived from ground-based data collected at Barrow, Alaska, *Journal of Climate*,  
892 16, 445-461, 2003.

893 Drozd, G., Woo, J., Häkkinen, S. A. K., Nenes, A., and McNeill, V. F.: Inorganic salts  
894 interact with oxalic acid in submicron particles to form material with low  
895 hygroscopicity and volatility, *Atmos. Chem. Phys.*, 14, 5205-5215, 2014.

896 Fairlie, T. D., Jacob, D. J., Dibb, J. E., Alexander, B., Avery, M. A., van Donkelaar,  
897 A., and Zhang, L.: Impact of mineral dust on nitrate, sulfate, and ozone in  
898 transpacific Asian pollution plumes, *Atmospheric Chemistry and Physics*, 10,  
899 3999-4012, 2010.

900 Falkovich, A. H., Ganor, E., Levin, Z., Formenti, P., and Rudich, Y.: Chemical and  
901 mineralogical analysis of individual mineral dust particles, *Journal of Geophysical  
902 Research-Atmospheres*, 106, 18029-18036, 2001.

903 Feingold, G., Cotton, W. R., Kreidenweis, S. M., and Davis, J. T.: The impact of giant  
904 cloud condensation nuclei on drizzle formation in stratocumulus: Implications for  
905 cloud radiative properties, *Journal of the Atmospheric Sciences*, 56, 4100-4117,  
906 1999.

907 Feng, Y. and Penner, J. E.: Global modeling of nitrate and ammonium: Interaction of  
908 aerosols and tropospheric chemistry, *Journal of Geophysical Research-*  
909 *Atmospheres*, 112, 2007.

910 Fountoukis, C. and Nenes, A.: Continued development of a cloud droplet formation  
911 parameterization for global climate models, *J. Geophys. Res.*, 110, doi:  
912 10.1029/2004JD005591, 2005.

913 Fountoukis, C. and Nenes, A.: ISORROPIA II: a computationally efficient  
914 thermodynamic equilibrium model for  $K^+$ - $Ca^{2+}$ - $Mg^{2+}$ - $NH_4^+$ - $Na^+$ - $SO_4^{2-}$ - $NO_3^-$ - $Cl^-$ -  
915  $H_2O$  aerosols, *Atmospheric Chemistry and Physics*, 7, 4639-4659, 2007.

916 Fountoukis, C., Nenes, A., Meskhidze, N., Bahreini, R., Conant, W. C., Jonsson, H.,  
917 Murphy, S., Sorooshian, A., Varutbangkul, V., Brechtel, F., Flagan, R. C., and  
918 Seinfeld, J. H.: Aerosol-cloud drop concentration closure for clouds sampled  
919 during the International Consortium for Atmospheric Research on Transport and  
920 Transformation 2004 campaign, *J. Geophys. Res.*, 112, doi:  
921 10.1029/2006JD007272, 2007.

922 Fountoukis, C., Nenes, A., Sullivan, A., Weber, R., Van Reken, T., Fischer, M.,  
923 Matias, E., Moya, M., Farmer, D., and Cohen, R. C.: Thermodynamic  
924 characterization of Mexico City aerosol during MILAGRO 2006, *Atmospheric*  
925 *Chemistry and Physics*, 9, 2141-2156, 2009.

926 Gantt, B., He, J., Zhang, X., Zhang, Y., and Nenes, A.: Incorporation of advanced  
927 aerosol activation treatments into CESM/CAM5: model evaluation and impacts on  
928 aerosol indirect effects, *Atmospheric Chemistry and Physics*, 14, 7485-7497, 2014.

929 Ganzeveld, L. N., Lelieveld, J., Dentener, F. J., Krol, M. C., Bouwman, A. J., and  
930 Roelofs, G. J.: Global soil-biogenic NO<sub>x</sub> emissions and the role of canopy  
931 processes, *Journal of Geophysical Research-Atmospheres*, 107, 2002.

932 Garimella, S., Huang, Y. W., Seewald, J. S., and Cziczo, D. J.: Cloud condensation  
933 nucleus activity comparison of dry- and wet-generated mineral dust aerosol: the  
934 significance of soluble material, *Atmospheric Chemistry and Physics*, 14, 6003-  
935 6019, 2014.

936 Giannadaki, D., Pozzer, A., and Lelieveld, J.: Modeled global effects of airborne  
937 desert dust on air quality and premature mortality, *Atmospheric Chemistry and*  
938 *Physics*, 14, 957-968, 2014.

939 Grewe, V., Brunner, D., Dameris, M., Grenfell, J. L., Hein, R., Shindell, D., and  
940 Staehelin, J.: Origin and variability of upper tropospheric nitrogen oxides and  
941 ozone at northern mid-latitudes, *Atmospheric Environment*, 35, 3421-3433, 2001.

942 Grini, A., Myhre, G., Zender, C. S., and Isaksen, I. S. A.: Model simulations of dust  
943 sources and transport in the global atmosphere: Effects of soil erodibility and wind  
944 speed variability, *J. Geophys. Res.*, 110, doi: 10.1029/2004JD005037, 2005.

945 Gustafsson, R. J., Orlov, A., Badger, C. L., Griffiths, P. T., Cox, R. A., and Lambert,  
946 R. M.: A comprehensive evaluation of water uptake on atmospherically relevant  
947 mineral surfaces: DRIFT spectroscopy, thermogravimetric analysis and aerosol  
948 growth measurements, *Atmospheric Chemistry and Physics*, 5, 3415-3421, 2005.

949 Hatch, C. D., Greenaway, A. L., Christie, M. J., and Baltrusaitis, J.: Water adsorption  
950 constrained Frenkel-Halsey-Hill adsorption activation theory: Montmorillonite and  
951 illite, *Atmospheric Environment*, 87, 26-33, 2014.

952 Hauglustaine, D. A., Balkanski, Y., and Schulz, M.: A global model simulation of  
953 present and future nitrate aerosols and their direct radiative forcing of climate,  
954 *Atmospheric Chemistry and Physics*, 14, 11031-11063, 2014.

955 Haywood, J. and Boucher, O.: Estimates of the direct and indirect radiative forcing  
956 due to tropospheric aerosols: A review, *Reviews of Geophysics*, 38, 513-543,  
957 2000.

958 Herich, H., Tritscher, T., Wiacek, A., Gysel, M., Weingartner, E., Lohmann, U.,  
959 Baltensperger, U., and Cziczo, D. J.: Water uptake of clay and desert dust aerosol  
960 particles at sub- and supersaturated water vapor conditions, *Phys. Chem. Chem.*  
961 *Phys.*, 11, 7804-7809, 2009.

962 IPCC: (Intergovernmental Panel on Climate Change): The physical science basis.  
963 Contribution of working group I to the fifth assessment report of the  
964 intergovernmental panel on climate change. T.F. Stocker, D. Qin, G.-K. Plattner,  
965 M. Tignor, S.K. Allen, J. Boschung, A. Nauels, Y. Xia, V. Bex, and P.M. Midgley  
966 (eds.). Cambridge University Press, Cambridge, United Kingdom and New York,  
967 NY, USA, 2013. 2013.

968 Jeuken, A. B. M., Siegmund, P. C., Heijboer, L. C., Feichter, J., and Bengtsson, L.:  
969 On the potential of assimilating meteorological analyses in a global climate model  
970 for the purpose of model validation, *Journal of Geophysical Research-*  
971 *Atmospheres*, 101, 16939-16950, 1996.

972 Jöckel, P., Kerkweg, A., Pozzer, A., Sander, R., Tost, H., Riede, H., Baumgaertner,  
973 A., Gromov, S., and Kern, B.: Development cycle 2 of the Modular Earth  
974 Submodel System (MESSy2), *Geoscientific Model Development*, 3, 717-752,  
975 2010.

976 Jöckel, P., Tost, H., Pozzer, A., Bruehl, C., Buchholz, J., Ganzeveld, L., Hoor, P.,  
977 Kerkweg, A., Lawrence, M. G., Sander, R., Steil, B., Stiller, G., Tanarhte, M.,  
978 Taraborrelli, D., Van Aardenne, J., and Lelieveld, J.: The atmospheric chemistry  
979 general circulation model ECHAM5/MESSy1: consistent simulation of ozone from  
980 the surface to the mesosphere, *Atmos. Chem. Phys.*, 6, 5067-5104, 2006.

981 Kalkavouras, P., Bossioli, E., Bezantakos, S., Bougiatioti, A., Kalivitis, N.,  
982 Stavroulas, I., Kouvarakis, G., Protonotariou, A. P., Dandou, A., Biskos, G.,  
983 Mihalopoulos, N., Nenes, A., and Tombrou, M.: New Particle Formation in the  
984 South Aegean Sea during the Etesians: importance for CCN production and cloud  
985 droplet number, *Atmos. Chem. Phys. Discuss.*, 2016, 1-35, 2016.

986 Kallos, G., Solomos, S., Kushta, J., Mitsakou, C., Spyrou, C., Bartsotas, N., and  
987 Kalogeri, C.: Natural and anthropogenic aerosols in the Eastern Mediterranean and  
988 Middle East: Possible impacts, *Science of the Total Environment*, 488, 391-399,  
989 2014.

990 Karydis, V. A., Capps, S. L., Russell, A. G., and Nenes, A.: Adjoint sensitivity of  
991 global cloud droplet number to aerosol and dynamical parameters, *Atmospheric*  
992 *Chemistry and Physics*, 12, 9041-9055, 2012.

993 Karydis, V. A., Kumar, P., Barahona, D., Sokolik, I. N., and Nenes, A.: On the effect  
994 of dust particles on global cloud condensation nuclei and cloud droplet number,  
995 *Journal of Geophysical Research-Atmospheres*, 116, ~~2011a~~,  
996 [Karydis, V. A., Tsimpidi, A. P., Lei, W., Molina, L. T., and Pandis, S. N.: Formation](#)  
997 [of semivolatile inorganic aerosols in the Mexico City Metropolitan Area during the](#)  
998 [MILAGRO campaign, \*Atmospheric Chemistry and Physics\*, 11, 13305-13323,](#)  
999 [2011b.](#)

1000 Karydis, V. A., Tsimpidi, A. P., Pozzer, A., Astitha, M., and Lelieveld, J.: Effects of  
1001 mineral dust on global atmospheric nitrate concentrations, *Atmos. Chem. Phys.*,  
1002 16, 1491-1509, 2016.

1003 Kelly, J. T., Chuang, C. C., and Wexler, A. S.: Influence of dust composition on cloud  
1004 droplet formation, *Atmos. Environ.*, 41, 2904-2916, 2007.

Formatted: Font: 12 pt

Formatted: Font: 12 pt

1005 Kerkweg, A., Buchholz, J., Ganzeveld, L., Pozzer, A., Tost, H., and Jöckel, P.:  
1006 Technical Note: An implementation of the dry removal processes DRY DEPosition  
1007 and SEDImentation in the Modular Earth Submodel System (MESSy), *Atmos.*  
1008 *Chem. Phys.*, 6, 4617-4632, 2006.

1009 Koch, D., Bauer, S. E., Del Genio, A., Faluvegi, G., McConnell, J. R., Menon, S.,  
1010 Miller, R. L., Rind, D., Ruedy, R., Schmidt, G. A., and Shindell, D.: Coupled  
1011 Aerosol-Chemistry-Climate Twentieth-Century Transient Model Investigation:  
1012 Trends in Short-Lived Species and Climate Responses, *Journal of Climate*, 24,  
1013 2693-2714, 2011.

1014 Koehler, K. A., Kreidenweis, S. M., DeMott, P. J., Petters, M. D., Prenni, A. J., and  
1015 Carrico, C. M.: Hygroscopicity and cloud droplet activation of mineral dust  
1016 aerosol, *Geophys. Res. Let.*, 36, doi: 10.1029/2009GL037348, 2009.

1017 Kumar, P., Nenes, A., and Sokolik, I. N.: Importance of adsorption for CCN activity  
1018 and hygroscopic properties of mineral dust aerosol, *Geophys. Res. Let.*, 36, doi:  
1019 10.1029/2009GL040827, 2009a.

1020 Kumar, P., Sokolik, I. N., and Nenes, A.: Cloud condensation nuclei activity and  
1021 droplet activation kinetics of wet processed regional dust samples and minerals,  
1022 *Atmos. Chem. Phys.*, 11, 8661-8676, 2011a.

1023 Kumar, P., Sokolik, I. N., and Nenes, A.: Measurements of cloud condensation nuclei  
1024 activity and droplet activation kinetics of fresh unprocessed regional dust samples  
1025 and minerals, *Atmos. Chem. Phys.*, 11, 3527-3541, 2011b.

1026 Kumar, P., Sokolik, I. N., and Nenes, A.: Parameterization of cloud droplet formation  
1027 for global and regional models: including adsorption activation from insoluble  
1028 CCN, *Atmos. Chem. Phys.*, 9, 2517-2532, 2009b.

1029 Kushta, J., Kallos, G., Astitha, M., Solomos, S., Spyrou, C., Mitsakou, C., and  
1030 Lelieveld, J.: Impact of natural aerosols on atmospheric radiation and consequent  
1031 feedbacks with the meteorological and photochemical state of the atmosphere,  
1032 *Journal of Geophysical Research-Atmospheres*, 119, 1463-1491, 2014.

1033 Laaksonen, A., Malila, J., Nenes, A., Hung, H. M., and Chen, J. P.: Surface fractal  
1034 dimension, water adsorption efficiency, and cloud nucleation activity of insoluble  
1035 aerosol, *Scientific Reports*, 6, 2016.

1036 Latham, T. L., Kumar, P., Nenes, A., Dufek, J., Sokolik, I. N., Trail, M., and Russell,  
1037 A.: Hygroscopic properties of volcanic ash, *Geophysical Research Letters*, 38,  
1038 2011.

1039 Leibensperger, E. M., Chen, W. T., Seinfeld, J. H., Nenes, A., Adams, P. J., Streets,  
1040 D. G., Kumar, N., and Rind, D.: Climatic Effects of 1950-2050 Changes in US  
1041 Anthropogenic Aerosols - Part 1: Aerosol trends and radiative forcing, *Atmo.*  
1042 *Chem. Phys.*, 2011. Submitted, 2011.

1043 Lelieveld, J., Evans, J. S., Fnais, M., Giannadaki, D., and Pozzer, A.: The contribution  
1044 of outdoor air pollution sources to premature mortality on a global scale, *Nature*,  
1045 525, 367-+, 2015.

1046 Levin, Z., Teller, A., Ganor, E., and Yin, Y.: On the interactions of mineral dust, sea-  
1047 salt particles, and clouds: A measurement and modeling study from the  
1048 Mediterranean Israeli Dust Experiment campaign, *J. Geophys. Res.*, 110, doi:  
1049 10.1029/2005JD005810, 2005.

1050 Liao, H., Adams, P. J., Chung, S. H., Seinfeld, J. H., Mickley, L. J., and Jacob, D. J.:  
1051 Interactions between tropospheric chemistry and aerosols in a unified general  
1052 circulation model, *Journal of Geophysical Research-Atmospheres*, 108, 2003.

1053 Lohmann, U. and Feichter, J.: Global indirect aerosol effects: a review, *Atmospheric*  
1054 *Chemistry and Physics*, 5, 715-737, 2005.

1055 Lohmann, U., Feichter, J., Chuang, C. C., and Penner, J. E.: Prediction of the number  
1056 of cloud droplets in the ECHAM GCM, *Journal of Geophysical Research-*  
1057 *Atmospheres*, 104, 9169-9198, 1999a.

1058 [Lohmann, U. and Ferrachat, S.: Impact of parametric uncertainties on the present-day  
1059 climate and on the anthropogenic aerosol effect, \*Atmos. Chem. Phys.\*, 10, 11373-  
1060 11383, 2010.](#)

1061 [Lohmann, U.,](#) McFarlane, N., Levkov, L., Abdella, K., and Albers, F.: Comparing  
1062 different cloud schemes of a single column model by using mesoscale forcing and  
1063 nudging technique, *Journal of Climate*, 12, 438-461, 1999b.

1064 Ma, J., Chen, Y., Wang, W., Yan, P., Liu, H., Yang, S., Hu, Z., and Lelieveld, J.:  
1065 Strong air pollution causes widespread haze-clouds over China, *Journal of*  
1066 *Geophysical Research-Atmospheres*, 115, 2010.

1067 Martin, G. M., Johnson, D. W., and Spice, A.: The measurements and  
1068 Parameterization of Effective Radius of Droplets in Warm Stratocumulus Clouds,  
1069 *Journal of the Atmospheric Sciences*, 51, 1823-1842, 1993.

1070 Martin, R. V., Jacob, D. J., Yantosca, R. M., Chin, M., and Ginoux, P.: Global and  
1071 regional decreases in tropospheric oxidants from photochemical effects of aerosols,  
1072 *Journal of Geophysical Research-Atmospheres*, 108, 2003.

1073 [Meskhidze, N., Nenes, A., Conant, W. C., and Seinfeld, J. H.: Evaluation of a new  
1074 cloud droplet activation parameterization with in situ data from CRYSTAL-FACE  
1075 and CSTRIFE, \*J. Geophys. Res.\*, 110, doi: 10.1029/2004JD005703, 2005.](#)

1076 [Morales, R. and Nenes, A.: Characteristic updrafts for computing distribution-  
1077 averaged cloud droplet number and stratocumulus cloud properties, \*J. Geophys.\*  
1078 \*Res.\*, 115, doi: 10.1029/2009JD013233, 2010.](#)

1079 [Morales, R., Nenes, A., Jonsson, H., Flagan, R. C., and Seinfeld, J. H.: Evaluation of  
1080 an entraining droplet activation parameterization using in situ cloud data, \*Journal\*  
1081 \*of Geophysical Research-Atmospheres\*, 116, 2011.](#)

1082 [Nenes, A. and Seinfeld, J. H.: Parameterization of cloud droplet formation in global  
1083 climate models, \*J. Geophys. Res.\*, 108, doi: 10.1029/2002JD002911, 2003.](#)

1084 Perry, K. D., Cliff, S. S., and Jimenez-Cruz, M. P.: Evidence for hygroscopic mineral  
1085 dust particles from the Intercontinental Transport and Chemical Transformation  
1086 Experiment, *Journal of Geophysical Research-Atmospheres*, 109, 2004.

1087 Petters, M. D. and Kreidenweis, S. M.: A single parameter representation of  
1088 hygroscopic growth and cloud condensation nucleus activity, *Atmospheric*  
1089 *Chemistry and Physics*, 7, 1961-1971, 2007.

1090 Pozzer, A., de Meij, A., Pringle, K. J., Tost, H., Doering, U. M., van Aardenne, J., and  
1091 Lelieveld, J.: Distributions and regional budgets of aerosols and their precursors  
1092 simulated with the EMAC chemistry-climate model, *Atmos. Chem. Phys.*, 12, 961-  
1093 987, 2012.

1094 Pozzer, A., Jockel, P., and Van Aardenne, J.: The influence of the vertical distribution  
1095 of emissions on tropospheric chemistry, *Atmospheric Chemistry and Physics*, 9,  
1096 9417-9432, 2009.

1097 Pozzer, A., Joeckel, P. J., Sander, R., Williams, J., Ganzeveld, L., and Lelieveld, J.:  
1098 Technical note: the MESSy-submodel AIRSEA calculating the air-sea exchange of  
1099 chemical species, *Atmos. Chem. Phys.*, 6, 5435-5444, 2006.

1100 Pringle, K. J., Tost, H., Message, S., Steil, B., Giannadaki, D., Nenes, A., Fountoukis,  
1101 C., Stier, P., Vignati, E., and Lelieveld, J.: Description and evaluation of GMXe: a  
1102 new aerosol submodel for global simulations (v1), *Geoscientific Model*  
1103 *Development*, 3, 391-412, 2010.

Formatted: Font: 12 pt

Formatted: Font: 12 pt

Formatted: Font: 12 pt

1104 Rausch, J., Heidinger, A., and Bennartz, R.: Regional assessment of microphysical  
1105 properties of marine boundary layer cloud using the PATMOS-x dataset, *J.*  
1106 *Geophys. Res.*, 115, doi: 10.1029/2010JD014468, 2010.

1107 Roberts, G., Mauger, G., Hadley, O., and Ramanathan, V.: North American and Asian  
1108 aerosols over the eastern Pacific Ocean and their role in regulating cloud  
1109 condensation nuclei, *Journal of Geophysical Research-Atmospheres*, 111, 2006.

1110 Röckner, E., Brokopf, R., Esch, M., Giorgetta, M., Hagemann, S., Kornbluh, L.,  
1111 Manzini, E., Schlese, U., and Schulzweida, U.: Sensitivity of simulated climate to  
1112 horizontal and vertical resolution in the ECHAM5 atmosphere model, *J. Climate*,  
1113 19, 3771-3791, 2006.

1114 Rosenfeld, D., Clavner, M., and Nirel, R.: Pollution and dust aerosols modulating  
1115 tropical cyclones intensities, *Atmospheric Research*, 102, 66-76, 2011.

1116 Sander, R., Baumgaertner, A., Gromov, S., Harder, H., Joeckel, P., Kerkweg, A.,  
1117 Kubistin, D., Regelin, E., Riede, H., Sandu, A., Taraborrelli, D., Tost, H., and Xie,  
1118 Z. Q.: The atmospheric chemistry box model CAABA/MECCA-3.0, *Geoscientific*  
1119 *Model Development*, 4, 373-380, 2011.

1120 Schwartz, S. E.: Cloud droplet nucleation and its connection to aerosol properties. In:  
1121 *Nucleation and Atmospheric Aerosols*, Wagner, M. K. a. P. E. (Ed.), Elsevier,  
1122 Oxford, 1996.

1123 Seinfeld, J. H. and Pandis, S. N.: *Atmospheric Chemistry and Physics: From Air*  
1124 *Pollution to Climate Change*, John Wiley & Sons, Inc., Hoboken, New Jersey,  
1125 2006.

1126 Smoydzin, L., Teller, A., Tost, H., Fnais, M., and Lelieveld, J.: Impact of mineral dust  
1127 on cloud formation in a Saharan outflow region, *Atmospheric Chemistry and*  
1128 *Physics*, 12, 11383-11393, 2012.

1129 Sorjamaa, R. and Laaksonen, A.: The effect of H<sub>2</sub>O adsorption on cloud drop  
1130 activation of insoluble particles: a theoretical framework, *Atmospheric Chemistry*  
1131 *and Physics*, 7, 6175-6180, 2007.

1132 Sposito, G.: *The Chemistry of Soils*, Oxford university Press, 1989.

1133 Stone, E. A., Yoon, S.-C., and Schauer, J. J.: Chemical Characterization of Fine and  
1134 Coarse Particles in Gosan, Korea during Springtime Dust Events, *Aerosol and Air*  
1135 *Quality Research*, 11, 31-43, 2011.

1136 Sullivan, R. C., Guazzotti, S. A., Sodeman, D. A., and Prather, K. A.: Direct  
1137 observations of the atmospheric processing of Asian mineral dust, *Atmospheric*  
1138 *Chemistry and Physics*, 7, 1213-1236, 2007.

1139 Sullivan, R. C., Moore, M. J. K., Petters, M. D., Kreidenweis, S. M., Roberts, G. C.,  
1140 and Prather, K. A.: Effect of chemical mixing state on the hygroscopicity and  
1141 cloud nucleation properties of calcium mineral dust particles, *Atmospheric*  
1142 *Chemistry and Physics*, 9, 3303-3316, 2009.

1143 Tobo, Y., Zhang, D., Matsuki, A., and Iwasaka, Y.: Asian dust particles converted  
1144 into aqueous droplets under remote marine atmospheric conditions, *Proceedings of*  
1145 *the National Academy of Sciences of the United States of America*, 107, 17905-  
1146 17910, 2010.

1147 Tost, H., Jockel, P. J., Kerkweg, A., Sander, R., and Lelieveld, J.: Technical note: A  
1148 new comprehensive SCAVenging submodel for global atmospheric chemistry  
1149 modelling, *Atmos. Chem. Phys.*, 6, 565-574, 2006.

1150 Tsimpidi, A. P., Karydis, V. A., Pandis, S. N., and Lelieveld, J.: [Global-scale  
1151 combustion sources of organic aerosols: Sensitivity to formation and removal  
1152 mechanisms, \*Atmos. Chem. Phys. Discuss.\*, 2017, 1-38, 2017.](#)

1153 Tsimpidi, A. P., Karydis, V. A., Pandis, S. N., and Lelieveld, J.: Global combustion  
1154 sources of organic aerosols: model comparison with 84 AMS factor-analysis data  
1155 sets, *Atmos. Chem. Phys.*, 16, 8939-8962, 2016.  
1156 Tsimpidi, A. P., Karydis, V. A., Pozzer, A., Pandis, S. N., and Lelieveld, J.: ORACLE  
1157 (v1.0): module to simulate the organic aerosol composition and evolution in the  
1158 atmosphere, *Geoscientific Model Development*, 7, 3153-3172, 2014.  
1159 Twohy, C. H., Kreidenweis, S. M., Eidhammer, T., Browell, E. V., Heymsfield, A. J.,  
1160 Bansemer, A. R., Anderson, B. E., Chen, G., Ismail, S., DeMott, P. J., and Van den  
1161 Heever, S. C.: Saharan dust particles nucleate droplets in eastern Atlantic clouds,  
1162 *Geophys. Res. Lett.*, 36, doi: 10.1029/2008GL035846, 2009.  
1163 Twomey, S.: Pollution and planetary albedo, *Atmospheric Environment*, 8, 1251-  
1164 1256, 1974.  
1165 Twomey, S. and Wojciechowski, T. A.: Observations of the Geographical Variation  
1166 of Cloud Nuclei, *Journal of the Atmospheric Sciences*, 26, 684-688, 1968.  
1167 van der Werf, G. R., Randerson, J. T., Giglio, L., Collatz, G. J., Mu, M., Kasibhatla,  
1168 P. S., Morton, D. C., DeFries, R. S., Jin, Y., and van Leeuwen, T. T.: Global fire  
1169 emissions and the contribution of deforestation, savanna, forest, agricultural, and  
1170 peat fires (1997-2009), *Atmos. Chem. Phys.*, 10, 11707-11735, 2010.  
1171 Weber, R. J., Guo, H. Y., Russell, A. G., and Nenes, A.: High aerosol acidity despite  
1172 declining atmospheric sulfate concentrations over the past 15 years, *Nat. Geosci.*,  
1173 9, 282-+, 2016.  
1174 Wurzler, S., Reisin, T. G., and Levin, Z.: Modification of mineral dust particles by  
1175 cloud processing and subsequent effects on drop size distributions, *Journal of*  
1176 *Geophysical Research-Atmospheres*, 105, 4501-4512, 2000.  
1177 Xu, L. and Penner, J. E.: Global simulations of nitrate and ammonium aerosols and  
1178 their radiative effects, *Atmospheric Chemistry and Physics*, 12, 9479-9504, 2012.  
1179 Yamashita, K., Murakami, M., Hashimoto, A., and Tajiri, T.: CCN Ability of Asian  
1180 Mineral Dust Particles and Their Effects on Cloud Droplet Formation, *Journal of*  
1181 *the Meteorological Society of Japan*, 89, 581-587, 2011.  
1182 Yienger, J. J. and Levy, H.: Empirical-model of global soil-biogenic NOx emissions,  
1183 *Journal of Geophysical Research-Atmospheres*, 100, 11447-11464, 1995.  
1184 Yin, Y. and Chen, L.: The effects of heating by transported dust layers on cloud and  
1185 precipitation: a numerical study, *Atmos. Chem. Phys.*, 7, 3497-3505, 2007.  
1186 Zender, C. S. and Kwon, E. Y.: Regional contrasts in dust emission responses to  
1187 climate, *J. Geophys. Res.*, 110, doi: 10.1029/2004JD005501, 2005.  
1188 Zhang, Y., Zhang, X., Wang, K., He, J., Leung, L. R., Fan, J., and Nenes, A.:  
1189 Incorporating an advanced aerosol activation parameterization into WRF-CAM5:  
1190 Model evaluation and parameterization intercomparison, *Journal of Geophysical*  
1191 *Research-Atmospheres*, 120, 6952-6979, 2015.  
1192 Zhao, C. S., Tie, X. X., Brasseur, G., Noone, K. J., Nakajima, T., Zhang, Q., Zhang,  
1193 R. Y., Huang, M. Y., Duan, Y., Li, G. L., and Ishizaka, Y.: Aircraft measurements  
1194 of cloud droplet spectral dispersion and implications for indirect aerosol radiative  
1195 forcing, *Geophys. Res. Lett.*, 33, doi: 10.1029/2006GL026653, 2006.  
1196

Formatted: Font: 12 pt

**Table 1.** Comparison of simulated and observed (Karydis et. al., 2011, and the references therein) cloud droplet number concentrations.

Location	Lat.	Long.	Alt.	Time	Observation	Simulation
S. Pacific Ocean			PBL	Annual	40	23
S. Pacific Ocean	20S-35S	135W-175W	PBL	Annual	82	26
Eastern Pacific Ocean	29N-32N	120W-123W	450-850m	July	49-279	133
N. Pacific Ocean	41N	131W	<1500m	April	21-74	51
N. Pacific Ocean			PBL	Annual	64	59
W. of Canary Islands	32N	25W	PBL	July	17	115
N. Atlantic Ocean			PBL	Annual	89	112
S. Atlantic Ocean			PBL	Annual	67	51
S. Indian Ocean			PBL	Annual	42	29
West Australia (remote)	30S-40S	88E-103E	PBL	Annual	107	22
Beaufort Sea (Western Arctic Ocean)	72N-78N	154W-159W	202-1017m	June	178-365	25
Beaufort Sea (Western Arctic Ocean)	70.5N-73N	145N-147N	300-3000m	June	20-225	28
Beaufort Sea (Western Arctic Ocean)	65N-75N	130W-170W	400-4600m	April	48-77	39
Northeast Alaska coast	69N-71N	150W-158W	400-4000m	October	10-30	23
Yellow Sea (Eastern coast of China)	28N-31N	127E-131E	PBL	Annual	30-1000	764
SE Asia coast	10N-40N	105E-150E	PBL	Annual	186 (100-250)	522
NE Asia coast			PBL	Annual	129	768
N. America coast (Pacific)			PBL	Annual	96	91
N. America coast (Pacific)	15N-35N	115W-140W	PBL	Annual	159 (150-300)	190
S. America coast (Pacific)			PBL	Annual	77	75
S. America coast (Pacific)	8S-28S	70W-90W	PBL	Annual	182 (100-300)	186
N. Africa coast (Atlantic)			PBL	Annual	95	123
S. Africa coast (Atlantic)			PBL	Annual	95	107
S. Africa coast (Atlantic)	5S-25S	10W-15E	PBL	Annual	153 (130-300)	189
Eastern N. Atlantic Ocean	50N-55N	25W-30W	800-2200m	April	65-300	39
NW coast of Santa Maria, Azores	37N	25W	550-1000m	June	150 (74-192)	83
Canary Islands Vicinity	28N	16.5W	PBL	June-July	51-256	174
Canary Islands Vicinity	28N	16.5W	PBL	June-July	90-300	174
Atlantic Ocean (W. of Morocco)	34N	11W	PBL	July	77	114
Coast of Oregon	45.5N	124.5W	PBL	August	25-210	124
Key West, FL	24.5N	82W	PBL	July	268-560	318
Bay of Fundy, Nova Scotia, Canada	44N	66W	20-290m	August	61 (59-97)	246
Cornwall Coast (SW UK)	50N	5.5W	450-800m	February	130	602
British Isles, UK	55N	2.5W	Surface	April	172	287
British Isles, UK	51N	6W	Surface	October	119	71
British Isles, UK	53N	9.5W	Surface	December	96	318
SE coast of England	51.5N-52N	1.5E-2.5E	380-750m	September	151-249	1019
Indian Ocean (SW of India)	10S-10N	65E-75E	50-550m	February-March	100-500	520

**Table 1.** Continued

Location	Lat.	Long.	Alt.	Time	Observation	Simulation
Qinghai Province (Western China)	34N-37N	98E-103E	PBL	Annual	30-700	585
Beijing, China	37N-41N	113E-120E	PBL	Annual	30-1100	1185
NE China (East of Beijing)	39N-40N	117.5E-118.5E	1719-1931m	April-May	200-800	813
Hebei Province (Central Eastern China)	35N-40N	112E-119E	PBL	Annual	30-400	1150
Cumbria, N. England	54.5N	2.5W	Surface	March-April	100-2000	743
Cumbria, N. England	54.5N	2.5W	Surface	May	482-549	840
Koblenz, Germany	50N	7.5E	901-914hPa	May	675-900	1258
Koblenz, Germany	50N	7.5E	945hPa	October	965	1039
Northern Finland	68N	24E	342-572m	Annual	154 (30-610)	332
Kuopio, Finland	62.5N	27.5E	306m	August-November	138	1142
Northern Finland	68N	24E	342-572m	October-November	55-470	336
Cabauw, Netherland	51N	4.5E	PBL	May	180-360	946
Jungfrauoch, Switzerland	46.5N	7.5E	Surface	July-August	112-416	176
Barrow, AK	71.5N	156.5W	389-830m	August	56	47
Barrow, AK	71.5N	156.5W	431-736m	May	222	26
Barrow, AK	71.5N	156.5W	297-591m	June	121	31
Barrow, AK	71.5N	156.5W	393-762m	July	54	29
Barrow, AK	71.5N	156.5W	1059-1608m	September	81	23
Southern Great Plains, OK	36.5N	97.5W	795-1450m	Winter	265-281	341
Southern Great Plains, OK	36.5N	97.5W	343-1241m	Winter	244	341
Southern Great Plains, OK	36.5N	97.5W	985-1885m	Spring	200-219	384
Southern Great Plains, OK	36.5N	97.5W	671-1475m	Spring	203	537
Southern Great Plains, OK	36.5N	97.5W	1280-2200m	Summer	128-159	393
Southern Great Plains, OK	36.5N	97.5W	756-1751m	Summer	131	603
Southern Great Plains, OK	36.5N	97.5W	1030-1770m	Autumn	217-249	505
Southern Great Plains, OK	36.5N	97.5W	404-1183m	Autumn	276	642
Southern Great Plains, OK	36.5N	97.5W	900-800hPa	March	200 (100-320)	563
Southern Great Plains, OK	36.5N	97.5W	300-600m	April	650	1159
Southern Great Plains, OK	36.5N	97.5W	700-1200m	September-October	457	740
Cleveland, OH; Detroit, MI	40N-42.5N	80.5W-85W	300-1000m	August	320-1300	817
Central Ontario, Canada	50N	85W	<2500m	October	147 (119-173)	201
Central Ontario	50N	85W	2000-2100m	Summer	350-360	143
Central Ontario	50N	85W	1300m	Winter	190	112
Upper NY State	44N	75W	1500m	Autumn	240	583
State College, Pennsylvania	41N	78W	1000-1600m	October	388	551
Mount Gibbes, NC	35.5N	82W	Surface	Annual	238-754	392
Cape Kennedy, FL	28.5N	80.5W	600-2800m	August	250-330	134

**Table 2.** Statistical evaluation of EMAC CDNC against ~~74~~worldwide<sup>75</sup> observational datasets worldwide, derived from in situ measurements and satellite retrievals.

Site Type	Number of datasets	Mean Observed (cm <sup>-3</sup> )	Mean Simulated (cm <sup>-3</sup> )	MAGE (cm <sup>-3</sup> )	MB (cm <sup>-3</sup> )	NME (%)	NMB (%)	RMSE (cm <sup>-3</sup> )
Clean marine	14	86	53	51	-33	60	-39	81
Polluted marine	24	169	296	159	127	94	75	263
Continental	37	339	536	269	198	80	58	358
<b>Total</b>	<b>75</b>	<b>237</b>	<b>369</b>	<b>193</b>	<b>132</b>	<b>82</b>	<b>56</b>	<b>295</b>

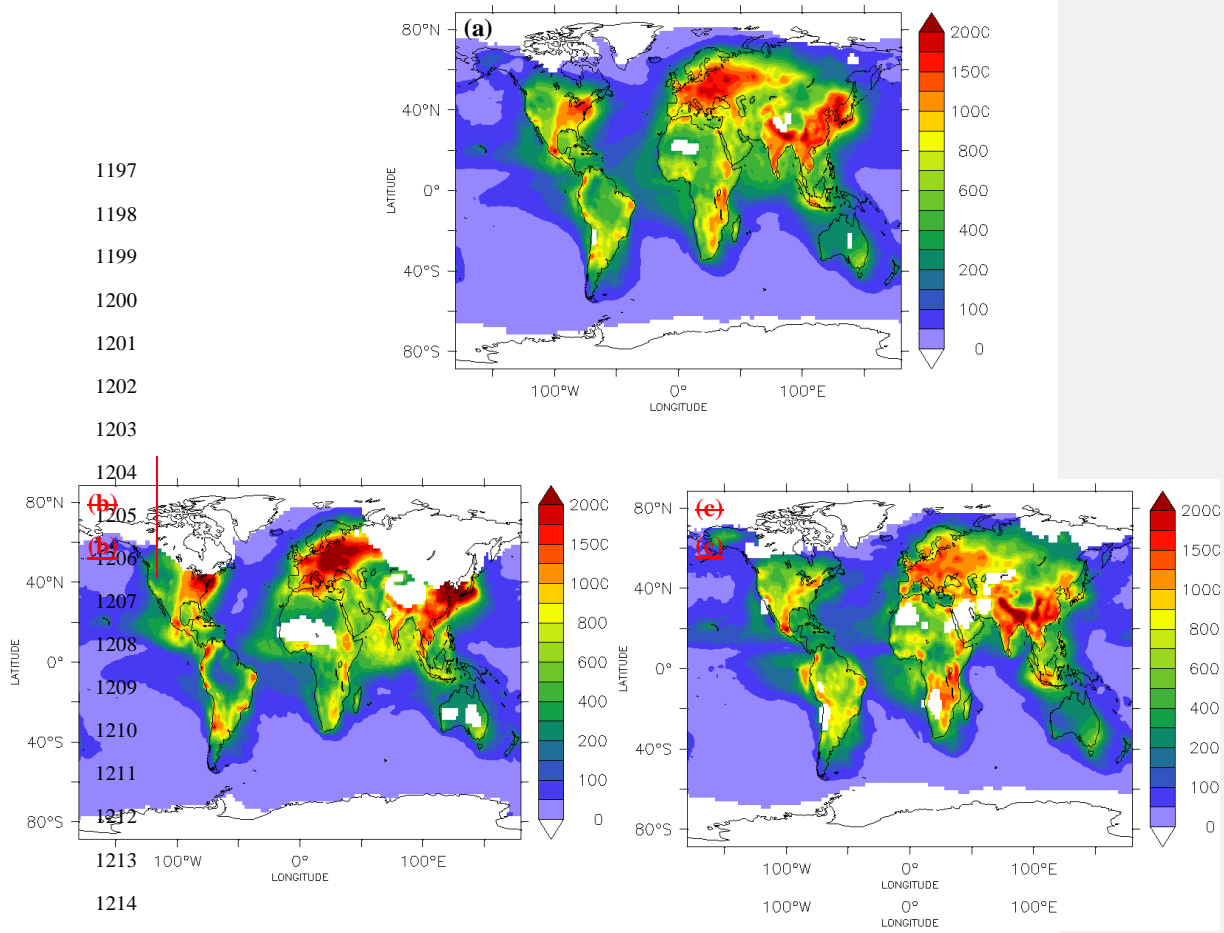


**Figure 1:** Predicted in-cloud (a) annual, (b) DJF, and (c) JJA mean cloud droplet number concentrations ( $\text{cm}^{-3}$ ) at the lowest cloud-forming level (940 mbhPa). White color represents areas that are cloud-free or covered by ice clouds.

1227

1228

1229

1230

1231

1232

1233

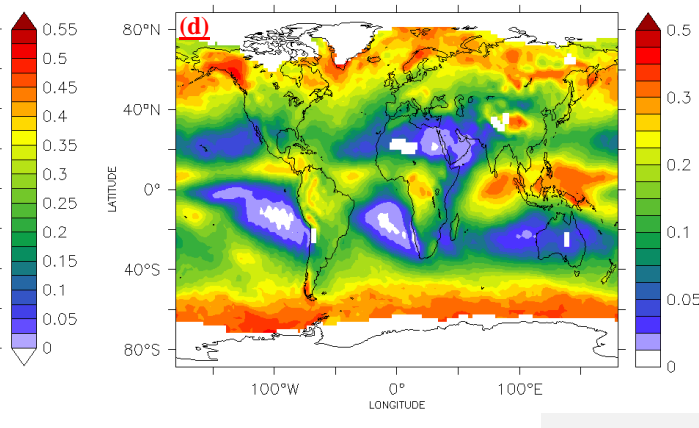
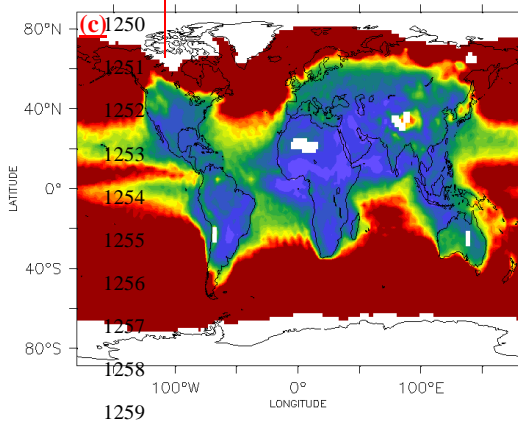
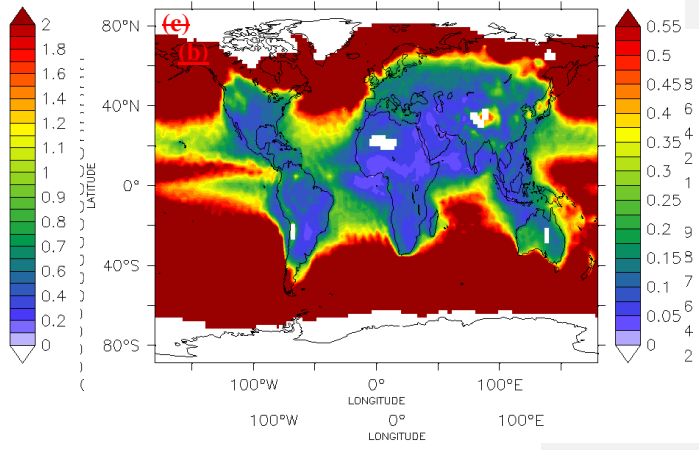
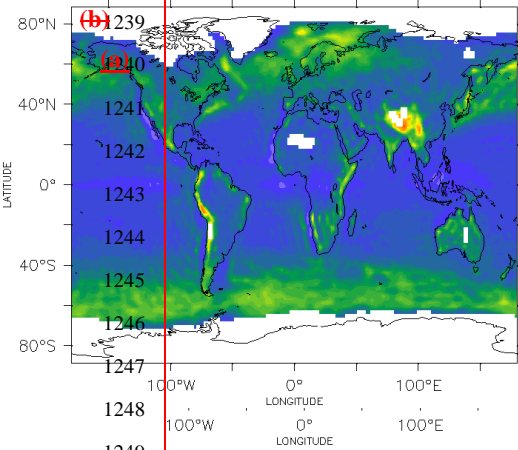
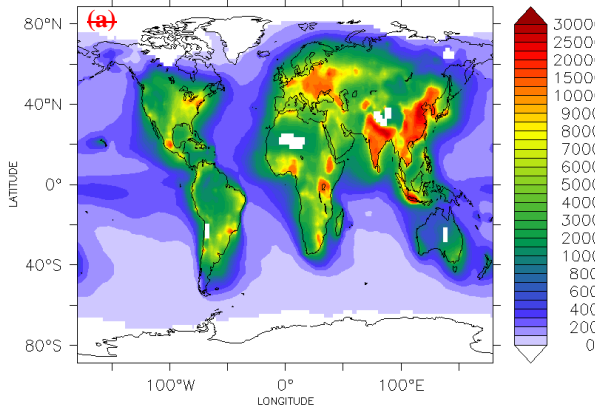
1234

1235

1236

1237

1238



1260 **Figure 2:** Predicted in-cloud annual mean **(a)** aerosol number concentration ( $\text{cm}^{-3}$ ),  
1261 **(b)** ~~large-scale~~ cloud updraft velocity ( $\text{m s}^{-1}$ ), ~~and~~ **(c)** maximum supersaturation (%) at  
1262 the lowest cloud-forming level (940 ~~mb~~-hPa), and **(d)** predicted annual mean low-  
1263 level cloud cover. White areas correspond to regions where liquid cloud droplets do  
1264 not form.

1265

**Formatted:** Font: Not Bold, Pattern: Clear

Formatted: Font: Not Bold, Pattern: Clear

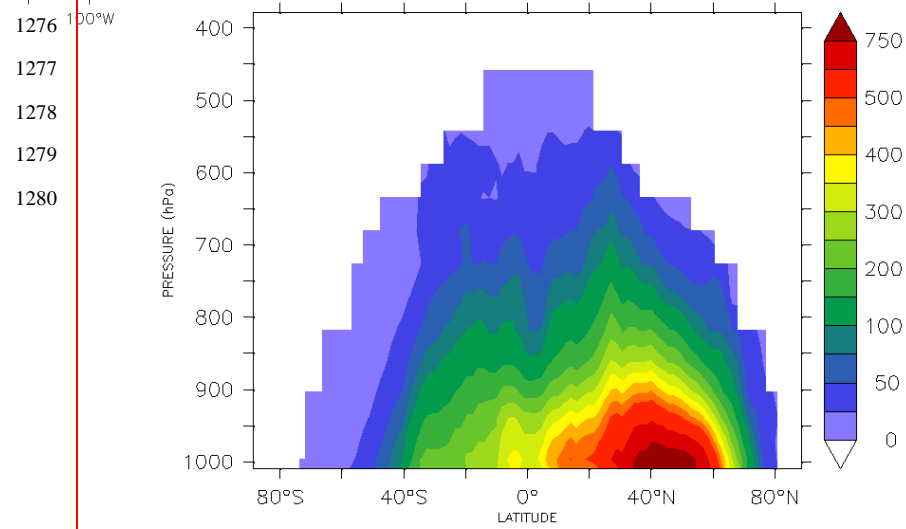
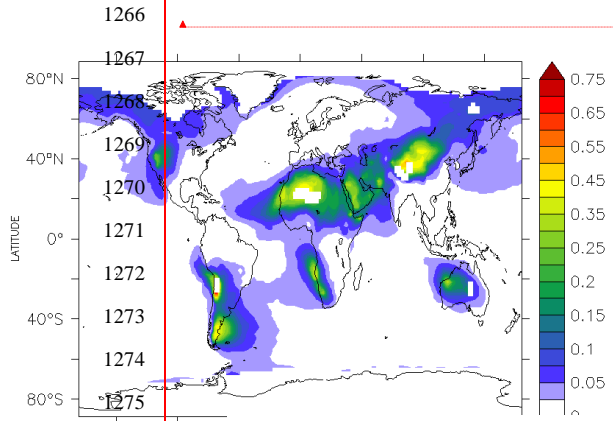
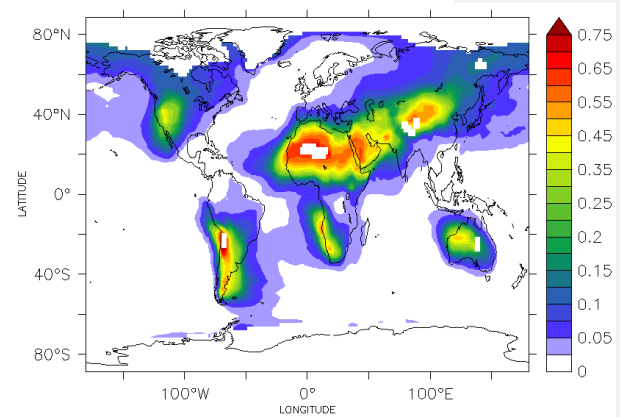


**Figure 3: Predicted**

1281  
1282  
1283  
1284  
1285  
1286  
1287  
1288  
1289  
1290  
1291  
1292  
1293  
1294  
1295



1296  
1297  
1298  
1299  
1300  
1301  
1302  
1303

---

**Figure 3:** Predicted annual mean insoluble fraction of aerosols in the (a) accumulation and (b) coarse modes at the lowest cloud-forming level (940 hPa).  
White areas correspond to regions where liquid cloud droplets do not form.

1304  
1305  
1306  
1307  
1308  
1309  
1310  
1311  
1312  
1313  
1314  
1315  
1316  
1317  
1318

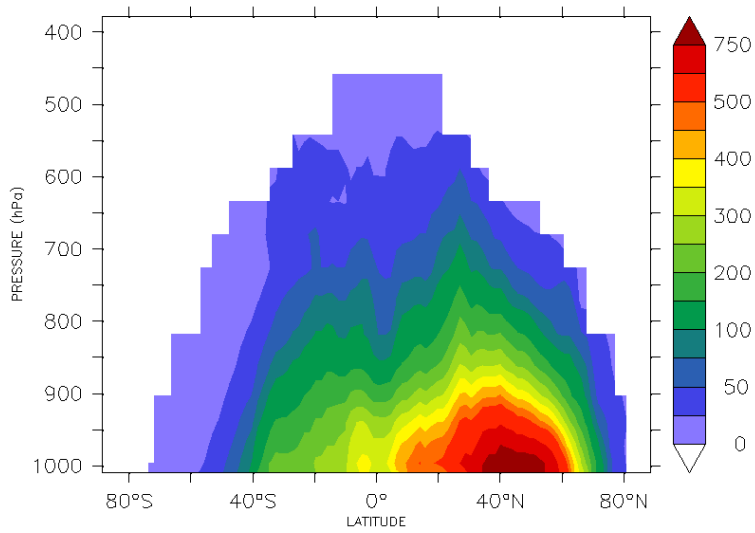


**Figure 4:** Predicted in-cloud zonal annual mean cloud droplet number concentration ( $\text{cm}^{-3}$ ). White areas correspond to regions where liquid cloud droplets do not form.

1319

Formatted: Line spacing: 1.5 lines

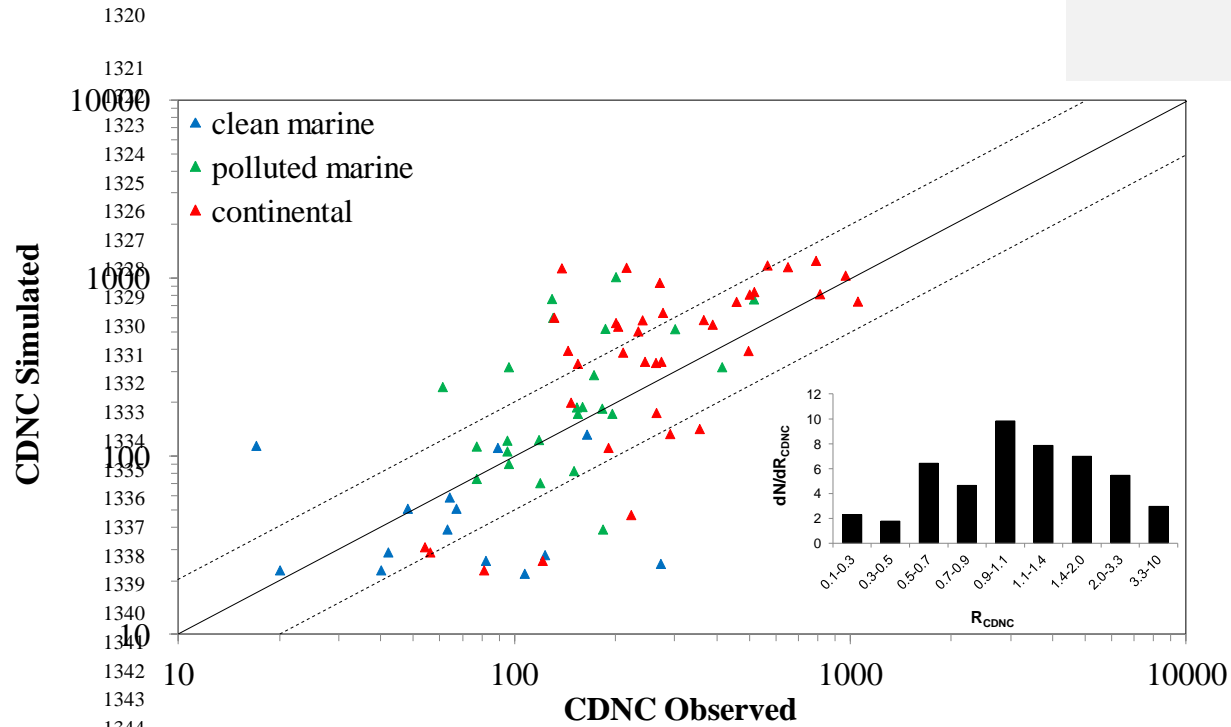
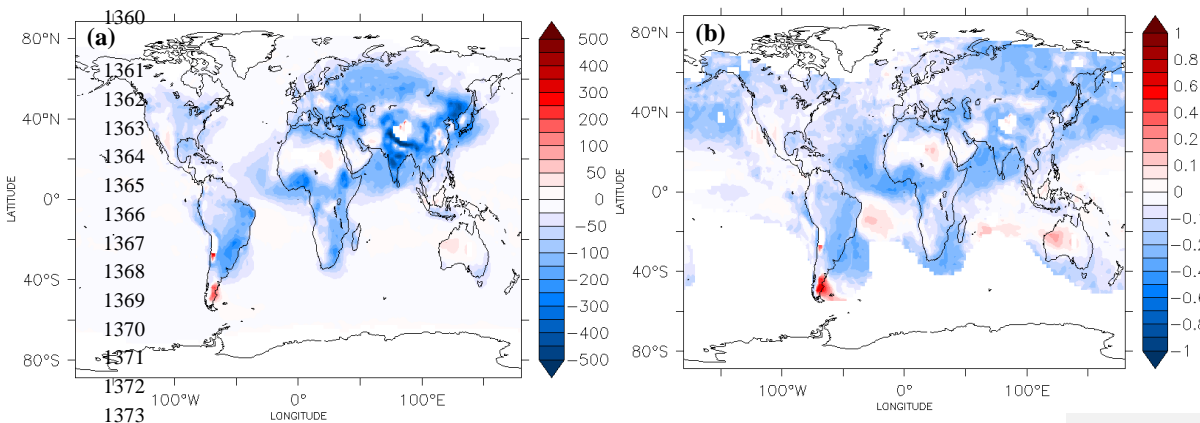


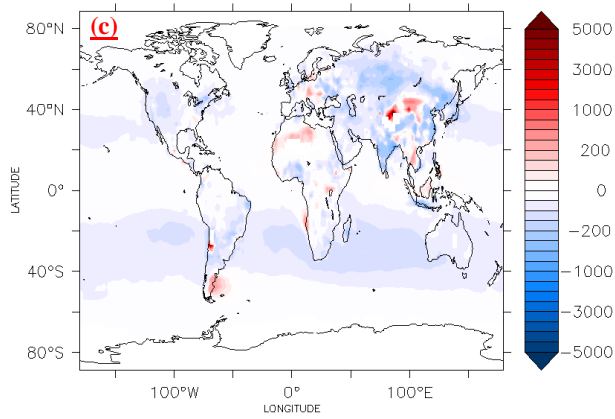
**Figure 45:** Scatterplot comparing model simulated cloud droplet number concentrations ( $\text{cm}^{-3}$ ) against ~~74~~<sup>75</sup> worldwide observational datasets worldwide, derived from in situ measurements and satellite retrievals. Also shown are the 1:1, 2:1, 1:2 lines, and the probability distribution of the ratio of the simulated CDNC to the observed CDNC ( $R_{CDNC}$ ), where N is the number of occurrences in each  $R_{CDNC}$  (inset plot).

Formatted: Line spacing: 1.5 lines

1355  
1356  
1357  
1358  
1359

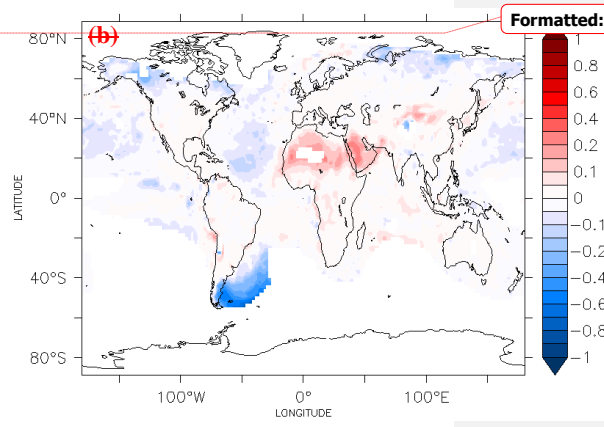
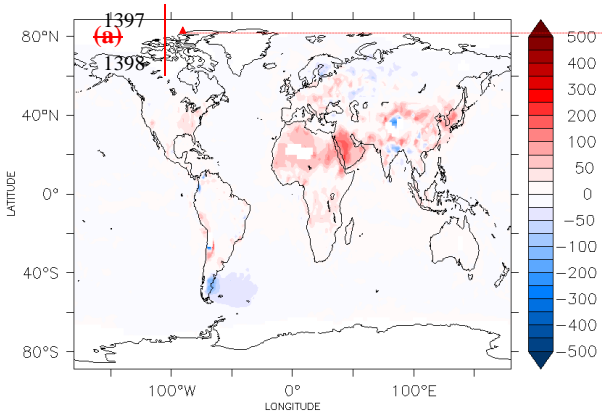


1372  
1373  
1374  
1375  
1376  
1377  
1378  
1379  
1380  
1381  
1382  
1383  
1384  
1385  
1386  
1387  
1388  
1389  
1390  
1391

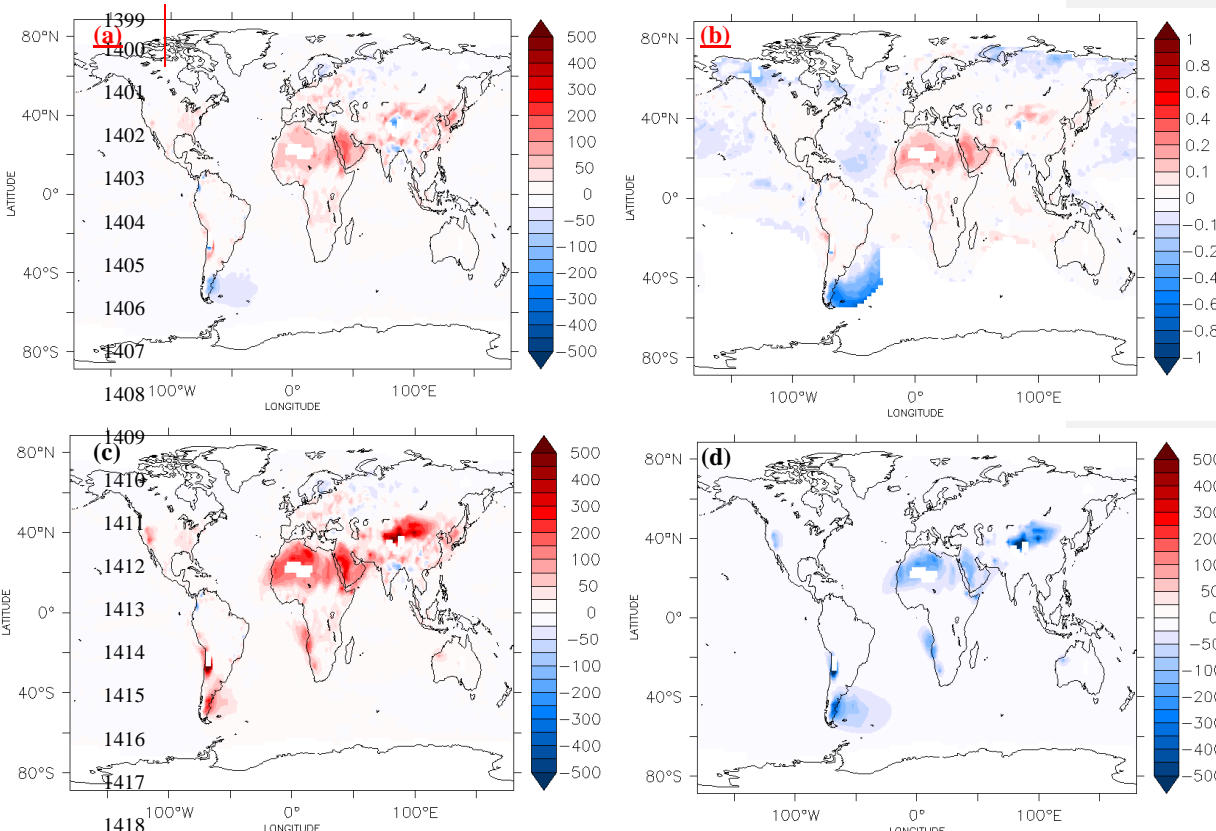


1392 **Figure 56:** (a) Absolute (in  $\text{cm}^{-3}$ ) and (b) fractional annual change of the predicted  
1393 CDNC, and (c) absolute (in  $\text{cm}^{-3}$ ) change of the predicted aerosol number  
1394 concentration (at the lowest cloud-forming level, 940 mbar) by switching on/off the  
1395 mineral dust emissions. A positive change corresponds to an increase from the  
1396 presence of dust.

Formatted: Justified, Line spacing: 1.5 lines



Formatted: Font: Not Bold, Pattern: Clear



1419  
 1420 | **Figure 67:** (a) Absolute (in  $\text{cm}^{-3}$ ) and (b) fractional annual average change of the  
 1421 | predicted total CDNC, and absolute (in  $\text{cm}^{-3}$ ) annual average change of the CDNC  
 1422 | from (c) soluble, and (d) insoluble particle modes, by switching on/off the mineral  
 1423 | dust chemistry. Concentrations reported at the lowest cloud-forming level (940  
 1424 | mbhPa). A positive change corresponds to an increase from dust-chemistry  
 1425 | interactions.

1426  
 1427  
 1428

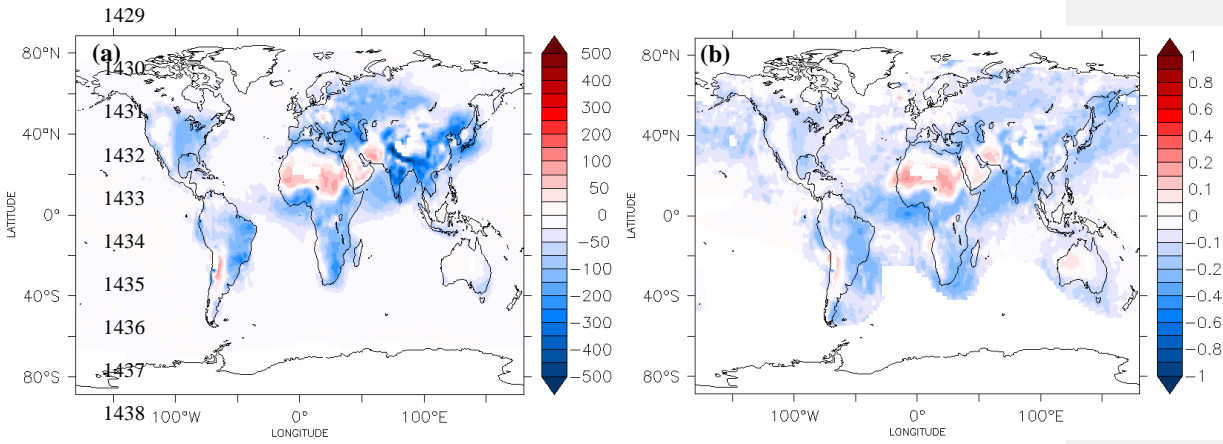


**Figure 78:** (a) Absolute (in  $\text{cm}^{-3}$ ) and (b) fractional annual average change of the predicted CDNC (at the lowest cloud-forming level, 940  $\text{mbhPa}$ ) by switching on/off the FHH adsorption activation physics. A positive change corresponds to an increase from water adsorption on mineral dust.

1439

1440

1441

1442

1443

1444

1445

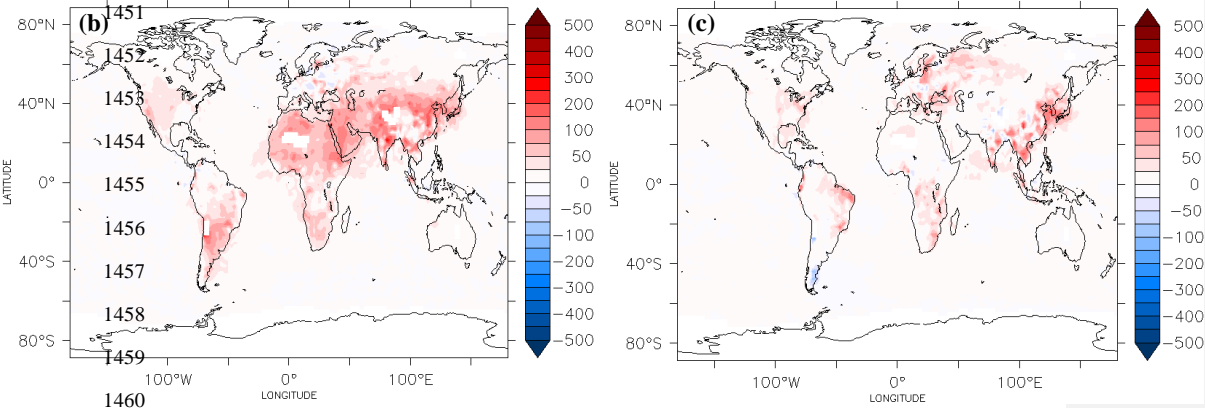
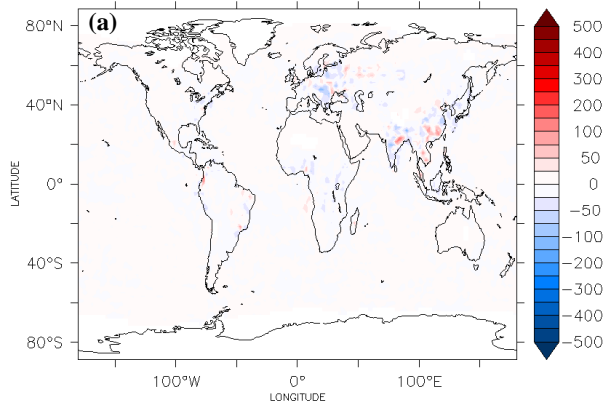
1446

1447

1448

1449

1450



1460

1461

1462 | **Figure 89:** Absolute changes (in  $\text{cm}^{-3}$ ) of the predicted annual average CDNC by (a)  
1463 assuming a globally uniform chemical composition of mineral dust, (b) increasing the  
1464  $B_{FHH}$  hydrophilicity parameter of dust by 10%, and (c) reducing mineral dust  
1465 emissions by 50%. A positive change corresponds to an increase relative to the  
1466 reference simulation.

Formatted: Line spacing: 1.5 lines